

EMBRITTLMENT SUSCEPTIBILITY OF
CORRODED PRE-STRESSING STEEL IN
CONCRETE DURING CATHODIC POLARIZATION

ARNAUD POEYDOMENGE

EMBRITTLEMENT SUSCEPTIBILITY
OF CORRODED PRE-STRESSING STEEL IN CONCRETE
DURING CATHODIC POLARIZATION

by

Arnaud Poeydomenge

A Thesis Submitted to the Faculty of
The College of Engineering
in Partial Fulfillment of the Requirements for the Degree of
Master of Science in Engineering

Florida Atlantic University

Boca Raton, Florida

August, 1997

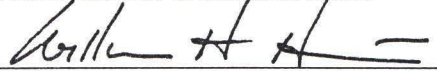
EMBRITTLMENT SUSCEPTIBILITY
OF CORRODED PRE-STRESSING STEEL IN CONCRETE
DURING CATHODIC POLARIZATION


by

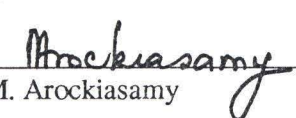
Arnaud Poeydomenge


This thesis was prepared under the direction of the candidate's thesis advisor, Dr. William H. Hartt, Department of Ocean Engineering, and has been approved by the members of his supervisory committee. It was submitted to the faculty of the College of Engineering and was accepted in partial fulfillment of the requirements for the degree of Master of Science in Engineering.

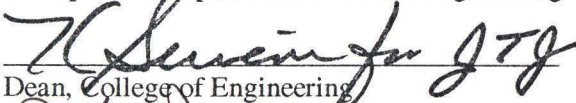
SUPERVISORY COMMITTEE:

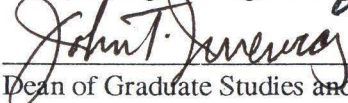

Thesis Advisor, Dr. William H. Hartt

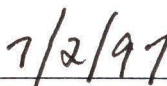

Dr. S. K. Lee


Dr. M. Arockiasamy


Chairperson, Department of Ocean Engineering


Dean, College of Engineering


Dean of Graduate Studies and Research


Date

Acknowledgments

I would like to take this opportunity to express my sincere appreciation to my thesis advisor, Dr. William H. Hartt, for his trust, constant availability and most valuable guidance throughout my research.

I would also like to thank George Jones and all the Graduate Students of the lab who made my stay in Florida both instructive and very pleasant.

Abstract

Author: Arnaud Poeydomenge
Title: Embrittlement Susceptibility of Corroded Pre-stressing Steel
in Concrete During Cathodic Polarization
Institution: Florida Atlantic University
Thesis Advisor: Dr. William H. Hartt
Degree: Master of Science in Engineering
Year: 1997

Experiments and analyses were performed to better define the limits of concern regarding hydrogen embrittlement in association with application of cathodic protection to prestressed concrete. To accomplish this, prestressed concrete specimens were locally corroded to different levels by anodic polarization and then polarized to $-1.30 V_{SCE}$. A procedure of examination was developed using strain gauges to determine the level of prestrain. Relatively few brittle failures of wires resulted due, at least in part, to a relatively low prestrain of the pretensioned tendons. A model was developed which, coupled with data from parallel research, permitted definition of the minimum cross section for brittle failure as a function of the magnitude of prestrain and corrosion morphology of the wire. These results were tabulated in a format that can be used during field inspection to identify structural elements for which fracture could occur upon application of cathodic protection.

Contents

	ACKNOWLEDGEMENTS.....	iii
	ABSTRACT.....	iv
	LIST OF FIGURES.....	viii
	LIST OF TABLES.....	x
1	INTRODUCTION.....	1
2	LITERATURE REVIEW.....	2
2.1	Pre-stressed concrete.....	2
2.2	Corrosion.....	2
2.3	Protection against corrosion.....	4
2.4	Hydrogen embrittlement (HE).....	6
2.5	Level of corrosion of a metallic specimen.....	9
2.6	Assessment of pre-stressed concrete corrosion damage.....	10
2.7	Stress in a pre-stressed beam.....	12
2.7.1	<i>Stress development in a pre-tensioned concrete beam.....</i>	<i>12</i>
2.7.2	<i>Stress loss of pre-stressing steel.....</i>	<i>12</i>
2.7.3	<i>Stress determination</i>	<i>14</i>
2.8	Objective of the research.....	14
3	EXPERIMENTAL PROCEDURE.....	15
3.1	Specimens.....	15
3.2	Computation of the strand development length.....	17
3.3	Polarization procedure and setup.....	18

3.4	Strain measurements.....	23
3.4.1	<i>Purpose and methodology.....</i>	23
3.4.2	<i>Principle and procedure of strain measurements.....</i>	23
3.4.3	<i>Strain gauge installation and measurement of tendon strain.....</i>	25
3.4.3.1	Strain gauge installation.....	25
3.4.3.2	Measurement of tendon strain	26
3.5	Tendon analysis.....	27
4	RESULTS AND DISCUSSION.....	28
4.1	Evaluation of strain measurements.....	28
4.2	Level of corrosion	30
4.2.1	<i>Specimens under anodic polarization</i>	30
4.2.2	<i>Drilled specimens under wet and dry cycle exposure.....</i>	36
4.3	Shape of corrosion pits.....	41
4.4	Strain measurements.....	42
4.5	Analysis of specimen pretension	48
4.6	Determination of the stress level in a corroded wire.....	49
4.6.1	<i>Computation of the tendon load</i>	49
4.6.2	<i>Theoretical model.....</i>	50
4.6.3	<i>Evaluation of data.....</i>	58
4.6.3.1	Calculations for specimen E5.....	58
4.6.3.2	Application to all the specimens.....	60
4.6.3.3	Analysis of the results	62
4.6.3.3.1	<i>Determination of the maximum possible stress.....</i>	62
4.6.3.3.2	<i>Validity of the corrosion model.....</i>	64
4.7	Stress state evaluation charts.....	66
4.7.1	<i>Simplified case where corrosion developed in one wire after another.....</i>	67

	4.7.2	<i>Application to tendons where corrosion developed in different wires at the same time.....</i>	70
5		CONCLUSION.....	73
		APPENDIX.....	74
		REFERENCES.....	77

List of figures

Figure 2-1: Pourbaix diagram for iron (all dissolved species at activities of 10^{-6} g-equiv/L).....	4
Figure 2-2: Evans diagram of corrosion of metal M.....	5
Figure 2-3: Influence of potential upon normalized CERT fracture load for smooth specimens....	8
Figure 2-4: Influence of potential upon normalized CERT fracture load for notched specimens...8	
Figure 2-5: Standard rating chart for pits.	11
Figure 2-6: Nomenclature of the stress development in a pre-stressed concrete specimen.....	13
Figure 3-1: Schematic illustration of a pre-stressed concrete beam specimen and sea water electrolyte pond.	16
Figure 3-2: Arrangement of the pre-stressed concrete beams.	20
Figure 3-3: Setup for three polarization test areas on a pre-stressed specimen.....	21
Figure 3-4: Polarization protocol.	22
Figure 3-5: Wheatstone bridge circuit.	25
Figure 4-1: Strain reading evolution as a function of the number of wires that had been cut in the central access.	29
Figure 4-2: Photograph of the broken wire from specimen C3-11.	33
Figure 4-3: Cup shape corrosion at the NE pond for beam E6.	39
Figure 4-4: Brittle fracture of tendon wire of specimen E6 at the SW pond.	39
Figure 4-5: Brittle fracture of tendon wire of specimen C3-6 at the SW pond.....	40
Figure 4-6: Brittle failure of tendon wire of specimen C3-6 at the SE pond.	40
Figure 4.7: Strain evolution during polarization of E9.	45

Figure 4-8: Strain evolution during polarization of E10.	46
Figure 4-9: Corrosion evolution with equal stress between wires in the corroded region.	55
Figure 4-10: Corrosion evolution with equal partial load in unsevered wires.	56
Figure 4-11: SSRT "Layer corrosion" specimens.	61
Figure 4-12: Number of specimens in each category for different numbers of remaining wires if $\epsilon_{\text{maximum}}$ is the computation reference.	64
Figure 4-13: Number of specimens in each category for different numbers of remaining wires if $\epsilon_{\text{minimum}}$ is the computation reference.	65

List of tables

Table 3-1: Concrete mix design and concrete properties.	17
Table 3-2: Computation results of the Development Length of the Pre-stressed Concrete Specimen.....	18
Table 4-1: Minimum remaining cross section of tendon wires in specimen C3-11.	33
Table 4-2: Minimum remaining cross section of tendon wires in specimen C3bas4.	34
Table 4-3: Minimum remaining cross section of tendon wires in specimens C3-9, E10 and E9...35	
Table 4-4: λ coefficient and minimum cross sections for specimens C 3-4, E 5, E 6, C 3-6 and C 3-1.....	37
Table 4-5: Prestrain measurement results.	44
Table 4-6: Summary of the stress computations based on maximum strain readings.	59
Table 4-7: Summary of the stress computations based on minimum strain readings.	60
Table 4-8: Results of SSRT experiments performed at $-1.3 V_{SCE}$	62
Table 4-9: Stress level and critical cross section for different levels of prestress and cross section reduction when the zone of minimum cross section of the wire can be compared to a smooth SSRT specimen.	67
Table 4-10: Stress level and critical cross section for different levels of prestress and cross section reduction when the zone of minimum cross section of the wire can be compared to a layer corrosion SSRT specimen.	68

1 INTRODUCTION

The main factor which compromises durability of reinforced concrete structures is corrosion of the embedded steel due to chloride exposure from either deicing salts or a marine environment. A recent survey [1] has reported that, mostly due to this phenomenon, 39 percent of the bridges in the United States are structurally deficient. Among protection techniques that can be employed to mitigate ongoing deterioration of concrete structures exposed to a chloride environment, cathodic protection (CP) is the most widely accepted. However, although engineers have been applying this technique successfully for years to reinforced concrete, reservations remain regarding its application to pre-stressed concrete because of the risk of hydrogen embrittlement (HE) [2]. In this regard, HE has been observed in high strength prestressing steels during cathodic polarization slow-strain-rate-testing (SSRT) experiments performed at potentials more negative than $-1,000 \text{ mV}_{\text{SCE}}$ using solutions which simulated a concrete environment [3-6]. Also, it has been projected that the more corroded a structure, the greater the probability that brittle fracture will result upon application of CP [7]; but there is presently no generally accepted technique whereby this can be quantitatively predicted. The objective of this research is to evaluate the risk of hydrogen embrittlement due to cathodic overprotection of actual pre-stressed concrete beams as a function of the corrosion level of the embedded tendon.

2 LITERATURE REVIEW

2.1 Pre-stressed concrete

Concrete is artificial rock obtained by mixing cement, water, aggregates of different size and admixtures. Resistance to compression is its main mechanical attribute (compressive strengths range from 25 to 60 Mpa). On the other hand, the strength of concrete in tension is typically an order of magnitude less than in compression [8]. To mitigate this weakness, steel rebars are incorporated into concrete in zones that are to be subjected to tension. The resultant composite material is termed *reinforced concrete*. In *pre-tensioned concrete*, zones that will have to support tension are compressed with high strength steel tendons. The latter are maintained under tension from external loading as the concrete sets, and this tension is released afterwards with transmission of the stress to the concrete. However, a fundamental problem with either reinforced or pre-stressed concrete is corrosion of embedded metal and reduction of the load bearing capacity.

2.2 Corrosion

Corrosion is an electrochemical degradation phenomenon. For a metal with n valence electrons, this process can be represented by the sum of two half cell reactions: oxidation



and reduction, either as



(or both) where reaction 2) corresponds to a neutral or alkaline environment and 3) to an acidic one.

Under certain conditions of pH and potential, which are illustrated in Figure 2.1 [9], iron may be passivated or protected by an oxide film. This film tends to be stable in an alkaline environment such as concrete where the pore water exhibits a pH of from 12.5 to 13.8, but it can locally break down if 1) the pH is decreased due to carbonation of the concrete (reaction between CO₂ from air in concrete pores with sodium, potassium and calcium hydroxides) or 2) chloride intrusion, as is common to marines environment and for deiced structures, occurs to above a threshold concentration at the steel depth combined with water and oxygen availability at cathodic sites [2, 10]. Consequently, pitting attack is promoted in these breakdown zones [11].

The two main consequences of corrosion in pre-stressed concrete are 1) a tensile stress in the concrete due to accumulation of solid corrosion products which cause cracks and spalls and 2) a reduction of the section area of the tendon. As the effective pre-stress in tendons is often specified as 70 percent of the ultimate tensile strength, a relatively modest reduction of the section area has been projected to result in fracture.

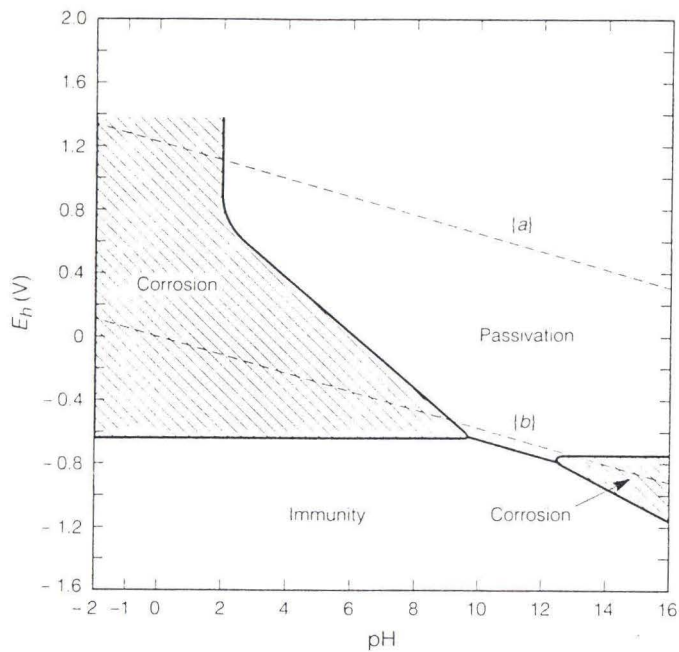


Figure 2-1: Pourbaix diagram for iron (all dissolved species at activities of 10^{-6} g-equiv/L).

2.3 Protection against corrosion

For a corroding steel bar, the anodic and cathodic processes (reactions 1-3) stabilize with time to a constant rate indicated by i_{corr} on Figure 2.2 [12]. If an applied current density, termed i_{app} , is imposed between an external electrode and the steel, the oxidation rate, i_a , is slowed ($i_a < i_{\text{corr}}$) while the corresponding rate for reduction, i_c , is increased ($i_c > i_{\text{corr}}$); and the potential is shifted to a more negative value. When the open circuit anodic potential (e_{M/M^+}) is reached, corrosion rate becomes nil. This is the principle of *cathodic protection* (CP). CP is recognized as the principally practiced technique for controlling corrosion of steel in chloride contaminated concrete [10, 13].

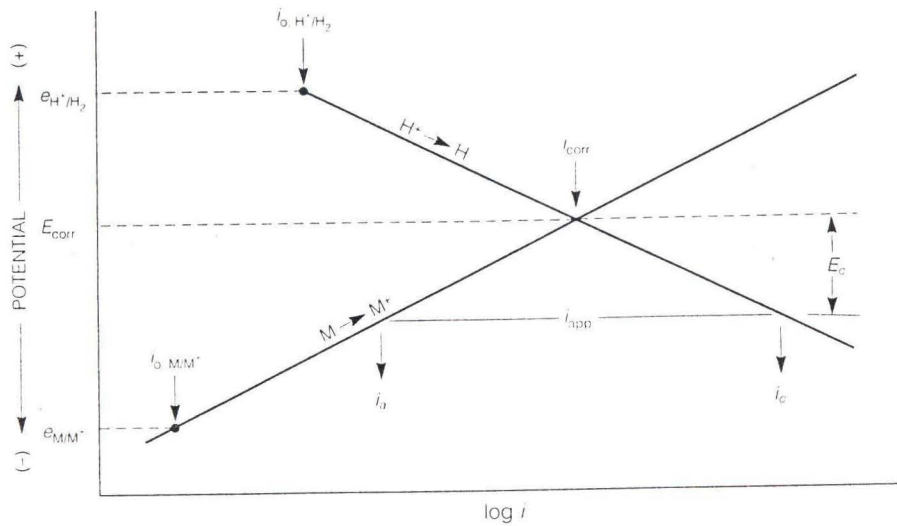


Figure 2-2: Evans diagram of corrosion of metal M.

The criteria described in the NACE Standard Recommended Practice [14] to judge effectiveness of cathodic protection of atmospherically exposed reinforced concrete structures are:

▷ 100 mV depolarization:

According to this criterion, the embedded steel is protected if, upon interruption of the protective current, the potential decay at active locations is by a minimum of 100 mV.

▷ Statistical distribution analysis:

This consists of conducting a potential survey of the reinforcement before energizing and computing the arithmetic mean potential, the most electronegative potential, and the standard deviation. Protection is stated to be achieved by application of a current such that the most electronegative potential of the reinforcement undergoes a negative shift equal to at least one standard deviation.

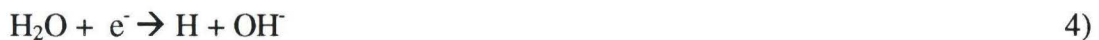
▷ E-log I analysis:

This procedure, which is most often used for determination of start-up current, is based on the definition of a straight line portion of the steel potential versus log applied current plot. The onset of this linearity defines the current that is specified for cathodic protection.

These criteria are considered to provide corrosion mitigation for reinforced concrete. Additionally, an operational criterion has to still be generally accepted for cathodic protection of prestressed concrete structures. This has been historically presented as a minimum potential that should not be exceeded such that hydrogen is not evolved. However, this concept remains open to debate.

2.4 Hydrogen embrittlement (HE)

When embedded steel is cathodically polarized to excessively negative potentials, part of the protective current may contribute to hydrogen formation; and the reaction



takes place at the steel/concrete interface [15]. The product hydrogen atoms can combine to form hydrogen gas or diffuse into the metal. Hydrogen entry can result in a loss of ductility and cause brittle cracking [15] termed *hydrogen embrittlement*. The mechanism(s) of this phenomenon is not clearly defined as of the present. Hydrogen can also react with carbon in steel at elevated temperatures to the detriment of strength and ductility [16].

In the strength range of pre-stressing steels the most susceptible microstructure is a *quenched and tempered* one followed by the *hot rolled pearlitic*, whereas the highest resistance against hydrogen-induced failure has been found in *cold drawn and stress relieved* steel [2].

Pre-corrosion of pre-stressing steel also influences susceptibility to HE. Different laboratories have performed slow strain rate testing (SSRT) in saturated $\text{Ca}(\text{OH})_2$ using smooth and notched specimens in order to determine the influence of pre-corrosion and applied potential on the mechanical properties of pre-stressing steel [3-6]. The smooth specimens were intended to represent uncorroded steel whereas notched ones simulated the more critical case where corrosion pits are present. As illustrated in Figures 2.3 and 2.4 [3-6], excessive overprotection (potentials more negative than $-1.20 V_{\text{SCE}}$) had only a minimal effect on smooth specimens in that the maximum load reduction was only about 10 percent. Other research showed that ultimate tensile stress at $-0.90 V_{\text{SCE}}$ or at $-1.30 V_{\text{SCE}}$ could be reduced by as much as 25 percent compared to strength in air for some smooth high strength steel specimens [17]; however, attempts to reproduce these results have not been successful. Most tests on notched specimens have indicated a risk of HE at potentials of $-1.00 V_{\text{SCE}}$ or more negative [15-17]. Using a 100 mV safety factor, this led to projection of $-0.90 V_{\text{SCE}}$ as a lower limit potential threshold. These results show the importance of local stress concentrations, as might arise from corrosion of the tendon, in affecting HE upon application of cathodic protection.

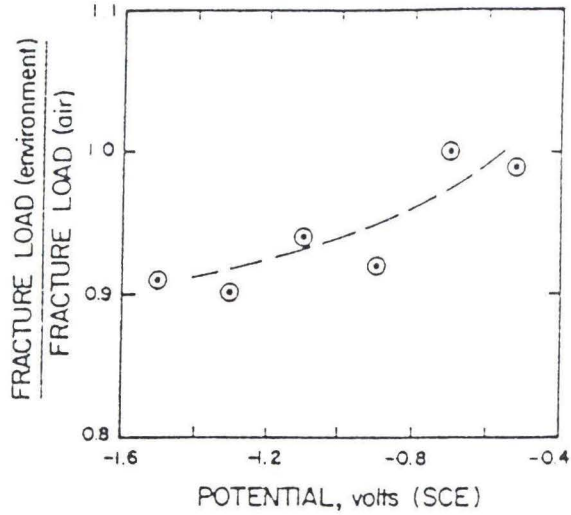


Figure 2-3: Influence of potential upon normalized CERT fracture load for smooth specimens.

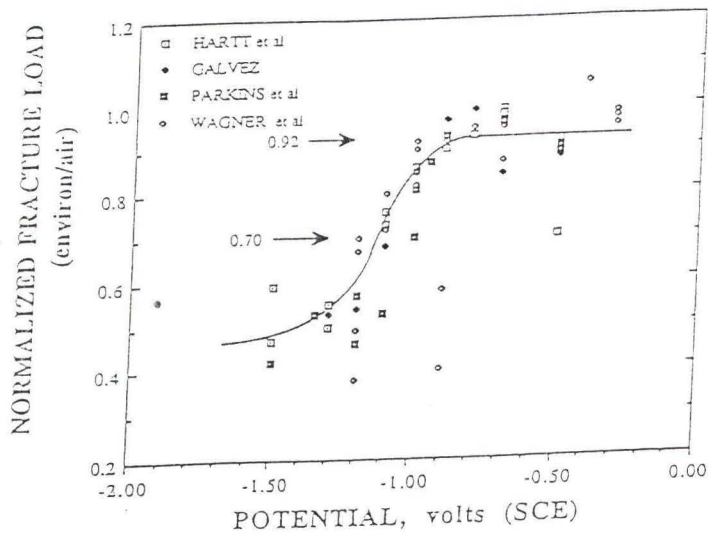


Figure 2-4: Influence of potential upon normalized CERT fracture load for notched specimens.

2.5 Level of corrosion of a metallic specimen

A guide has been defined by ASTM to examine and evaluate pitting corrosion [18].

The main techniques are:

° Nondestructive inspection according to one or more of the following:

Visual and microscopic inspection to determine surface width, shape, and density of pits.

Radiography, eddy currents, sonics or penetrants to detect irregularities of the sample.

Mass loss to give information about corrosion in general but this includes uniform and other forms of attack as well as pitting.

Micrometer or depth gage measurements to determine pit depth. This technique is often not useful, however, such as when pit undercutting has occurred.

Microscopical *focusing* into pits to measure the depth but this does not permit some shapes to be characterized.

° Complementary microscope inspection of a cross section of the pit to determine both depth and shape. However, this is a complicated technique; and the deepest pit is not always identified for sectioning from nondestructive visual inspection.

° Progressive machining of the most affected zone to survey a number of pits of different depths, including the pit of maximum depth.

Information regarding pitting can be expressed using standard charts such as the one in Figure 2.5 to code density, size, and depth. However, this is tedious and time consuming, recognizing that maximum values (depth, for example) usually have more significance

than the average. Data can also be expressed using the *pitting factor* which is the deepest metal penetration over the average. In conclusion, the means of identifying and evaluating pitting corrosion depend on the use that is to be made of the information; and one has to be certain that the selected parameter(s) reflects performance.

2.6 Assessment of pre-stressed concrete corrosion damage

Generally, in pre-stressed concrete structures, evidence of widespread corrosion related deterioration is not yet apparent [19]. Some non-intrusive methods such as the impact-echo are available for locating voids in bonded post-tensioning ducts, but this instrumentation is unable to detect whether a strand is corroded or broken. Also, some acoustic monitoring systems can provide continuous information about the time and location of strand failure [19]; but they require the installation of permanent sensors and dedicated data acquisition and processing systems. A cover-meter can also give an indication of the distance between the surface and any metallic product inside the concrete. However, this may be the embedded steel or metallic corrosion products that spread through the concrete; and such a device cannot detect a tendon failure.

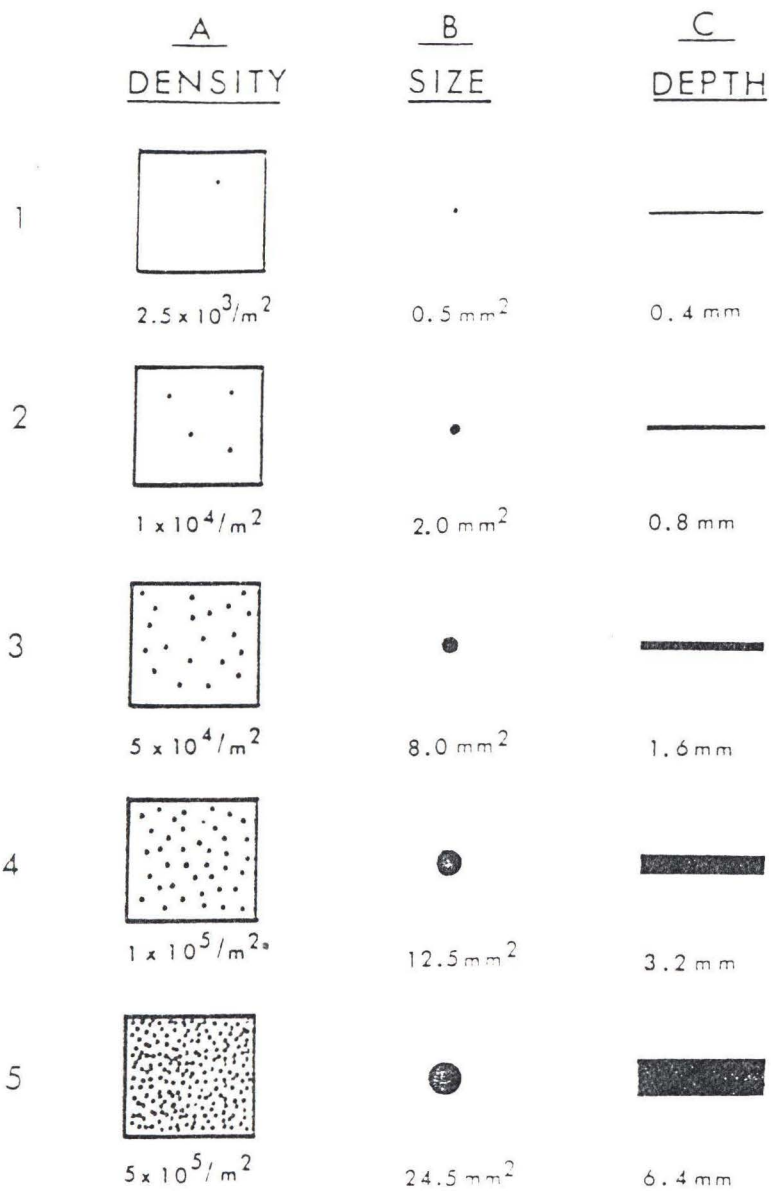


Figure 2-5: Standard rating chart for pits.

2.7 Stress in a pre-stressed beam

2.7.1 Stress development in a pre-tensioned concrete beam

As described in section 2.1, pre-tensioned steel tendons transfer load to the concrete by bond. The *transfer length* for a pre-stressing strand is the minimum embedment distance needed to prevent slip when the strand is loaded to the design stress [20]. The *development length* is comprised of the *transfer length* plus the *flexural bond length*, where bond stresses equilibrate the difference between the design stress and the effective pre-stress. Various equations for strand development length have been proposed by several organizations and laboratories, as summarized by Buckner [20]. The stress development in a pre-stressed concrete beam of constant rectangular cross section is represented in Figure 2.6, but it must be noted that the stress profile in the development length and the limit between transfer length and flexural bond length remain subject to debate. Also, while the stress in the central zone is illustrated as constant, it may, in fact, exhibit variations.

2.7.2 Stress loss of pre-stressing steel

In pre-stressed concrete the stress level should be reasonably well defined at the time of construction. However, over a period of approximately five years the following phenomena contribute to progressive reduction of pre-stressing force [21]:

1. Creep of concrete, which is a lateral flow or deformation due to the longitudinal compression force that counterbalances the effect of the tension in the tendon and which causes stress relaxation of the prestressing steel.
2. Drying shrinkage, due to the decrease in the volume of concrete as it loses moisture by evaporation.

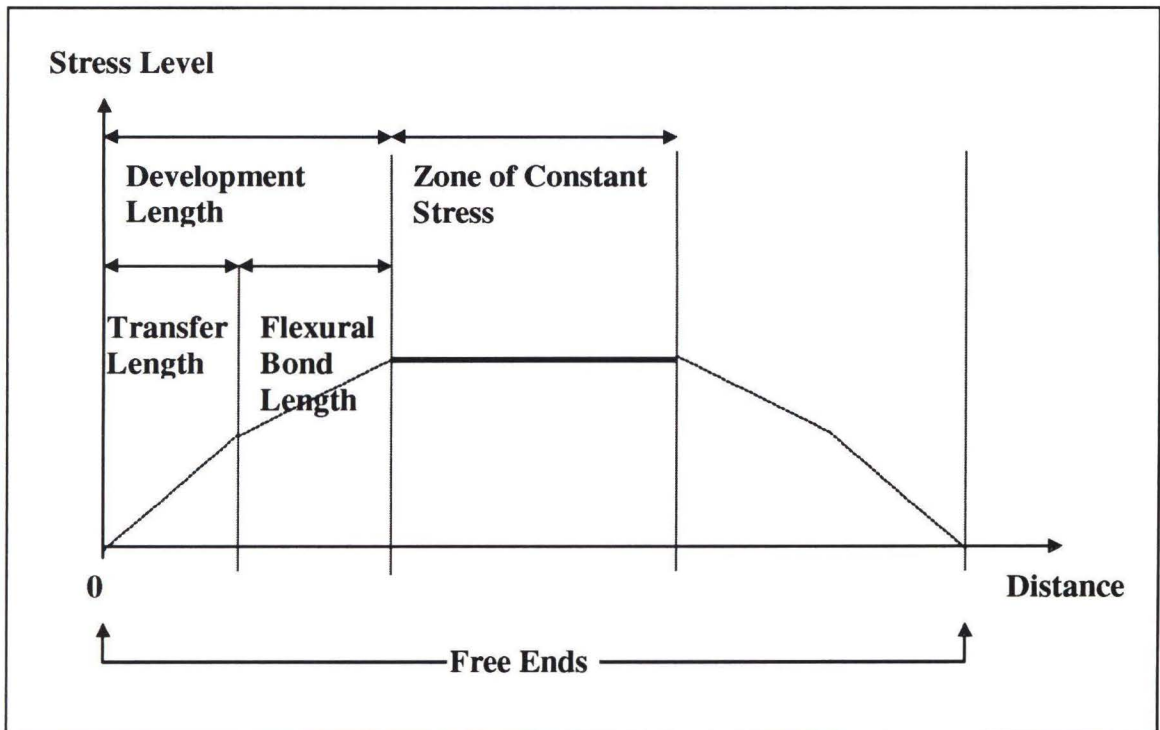


Figure 2-6: Nomenclature of the stress development in a pre-stressed concrete specimen.

Moreover, both the environment and the applied service load can contribute to stress losses that can not be nondestructively quantified due to the multiplicity of factors that are involved. Empirical estimation methods, which vary with the different codes of practice or recommendation, have been developed for the purpose of accomplishing this, however [21].

2.7.3 *Stress determination*

If stress relaxation exceeds a safety margin, failure can occur. Consequently, engineers are increasingly employing experimental techniques for determination of stress of in-service structures to provide condition assessment information. These methods can be destructive and impart some permanent damage to the tendons [22]. The required equipment that is employed for these assessments depends on the level of permanent damage that is acceptable, because processes that introduce the least damage generally require the highest accuracy and more sophisticated instrumentation.

2.8 Objective of the research

The question of the safety in the application of CP to prestressed concrete is of importance regarding the risk of this corrosion protection technique to induce embrittlement and fracture of corroded steel under tension. However, no specifications have yet been defined. The research results presented here intend to define criteria for application of CP to such structures while taking into account the levels of prestress and corrosion and to establish a field analysis method.

3 EXPERIMENTAL PROCEDURE

3.1 Specimens

Twenty three pre-tensioned concrete beam specimens were fabricated for the project at Curry Industries in Miami, Florida. These were 3 m long by 25 cm wide by 10-12 cm thick with two symmetrically positioned seven wire, nominally 11.11 mm diameter Grade 270 tendons. Each of the two tendons was pre-loaded to $103,600 \pm 500$ N in a 90 m-long pouring bed. The tendons were electrically isolated from one another, and no other steel was present in the pre-stressing bed forms. After pouring and finishing but prior to concrete setting, a 6 cm high by 20 cm wide by 2.1 m long rectangular polycarbonate frame ponding bath was positioned symmetrically upon the top surface of each specimen for subsequent sea water ponding. Figure 3.1 shows a schematic illustration of the specimen and bath. Concrete mix design parameters are listed in Table 3-1. The specimens were also locally admixed with chloride in three zones by adding 26 grams of solid CaCl_2 grains to the concrete at 7-8 cm wide positions, one at the center and the other two approximately 1 m from each end, during finishing. It was intended that a local Cl concentration of about 13 kg/m^3 (22 lb/yd^3) result from this.

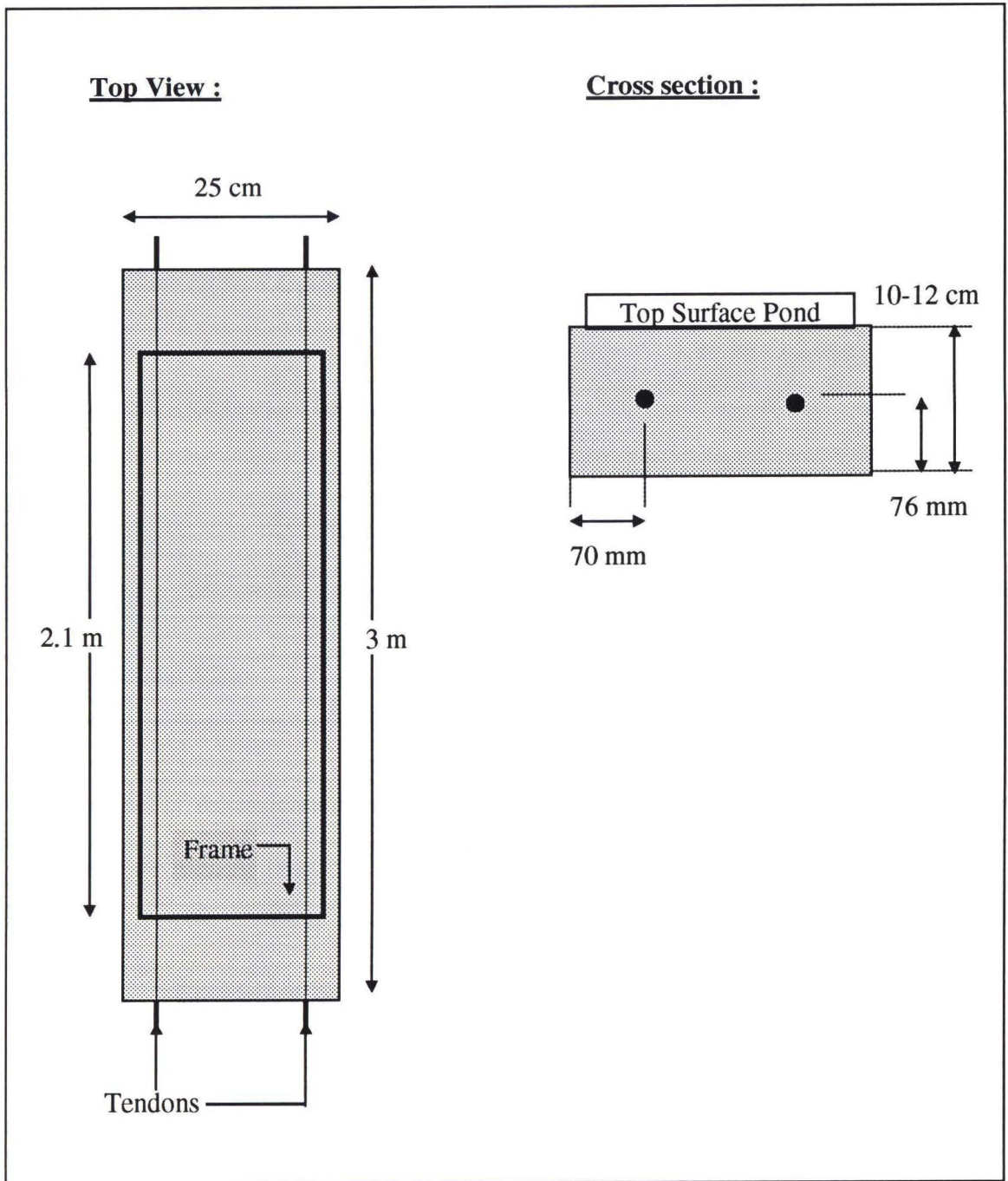


Figure 3-1: Schematic illustration of a pre-stressed concrete beam specimen and sea water electrolyte pond.

Table 3-1: Concrete mix design and concrete properties.

Cement (AASHTO M-85 Type I/II)	342.5 kg (755 lb.)
Coarse Aggregate (Grade 57 S.G. (SSO) 12.460)	771 kg (1700 lb.)
Fine Aggregate (2.86 S.G. (SSO) 12.560)	463.6 kg (1022 lb.)
Water Reducing Admixture (WRDA 72/AASHTO M-194 Type D)	1.44 kg (3.2 lb.)
Water	126.6 kg (279 lb./33.5 gal.)
Slump Range	0.0 to 8.9 cm (3.5 in.)
Air Content	3 to 6 %
Water / Cement Ratio	0.37

Each tendon in the specimens was designated as either “N” or “S”, depending on its position in the pouring bed.

3.2 Computation of the strand development length

The development length of prestressed concrete elements can be computed using various criteria and equations [20]. The specimen design was analyzed in terms of these, and the results are presented in Table 3-2. These show that the calculated development length extends approximately one-third of the beam from each end.

Table 3-2: Computation results of the development length of the pre-stressed concrete specimens.

Reference or Criterion	Equation (English units)	Development Length (inches - cm)
Current ACI/AASHTO [23,24]	$L_d = (f_{ps} - 2/3 f_{se}) \times d_b$ $= (270 - 160) \times 7/16 \times 0.438''$	$L_d = 21.08 \text{ in.}$ $= 53.54 \text{ cm}$
Zia & Mostafa's criterion [25]	$L_d = (1.5 \times f_{si} / f'_{ci} \times d_b - 4.6) + 1.25 \times (f_{su} - f_{se}) \times d_b$ $= (1.5 \times 189 / 4.0 \times 7/16 \times 0.438'' - 4.6) + 1.25 \times (270 - 160) \times 7/16 \times 0.438''$	$L_d = 35.33 \text{ in.}$ $= 89.74 \text{ cm}$
Martin and Scott equation [26]	$L_d = (d_b / 0.39) [f_{ps} - 135 / d_b^{1/6}]$ $= (7/16 \times 0.438'' / 0.39) [270 - 135 / (7/16 \times 0.438'')^{1/6}]$	$L_d = 45.30 \text{ in.}$ $= 115.06 \text{ cm}$
UTK Final Report [27]	$L_d = (f_{se} / 3 \times d_b + 1.42 \times (f_{ps} - f_{se}) \times d_b$ $= (160 / 3 \times 7/16 \times 0.438'' + 1.42 \times (270 - 160) \times 7/16 \times 0.438''$	$L_d = 40.15 \text{ in.}$ $= 101.98 \text{ cm}$

3.3 Polarization procedure and setup

After concrete setting, the pre-tensioned specimens were moved to the Laboratory for Marine Sciences and Engineering at the Gumbo Limbo Environmental Center and arranged as shown in Figure 3.2. In October, 1994 specimens began a sequential one week wet - one week dry sea water ponding cycle as described previously [28]. The acquired potential and corrosion rate data indicated that the level of corrosion after one year was not sufficient to cause HE during cathodic over-polarization. Subsequently, local areas of the zone of constant stress of the specimens were anodically polarized.

Beams selected for testing were equipped with up to three reduced area polycarbonate frame baths (approximately 10 cm long and traversing the beam width). In each case, the bath was positioned upon a CI admixed zone of the specimen. Figure 3.3 illustrates this setup schematically. Polarization was generated by a direct current rectifier (Good All Electric 24 V, 4 A) connected to the tendons and a catalyst coated titanium mesh (Elgard 210) positioned in the pond. The polarization was conducted in the current control mode with the zones on a particular specimen being powered in parallel. Once the intended amount of corrosion had transpired, cathodic polarization was applied for ten days by reversing the rectifier leads and powering such that an instant off potential of $-1.2 V_{SCE}$ or more negative was achieved to promote brittle fracture. Finally, an autopsy of the specimens was performed and the condition of the tendon assessed. Beams were tested sequentially using different anodic currents and times. The general procedure is illustrated in Figure 3.4. It was intended with the initial beams to establish a sufficiently high corrosion level that failure of the tendon would occur during cathodic over-protection and then to decrease the level of anodic polarization for subsequent beams until a threshold of corrosion below which failure did not occur during overprotection was determined. The corrosion level of the polarized specimens was defined in terms of a time-current parameter, $\sum_i [(I_i) \times (t_i)]$, where I_i is the applied anodic current (in mA) and t_i the application time (in days) for the period i .



Figure 3-2: Arrangement of the pre-stressed concrete beams.

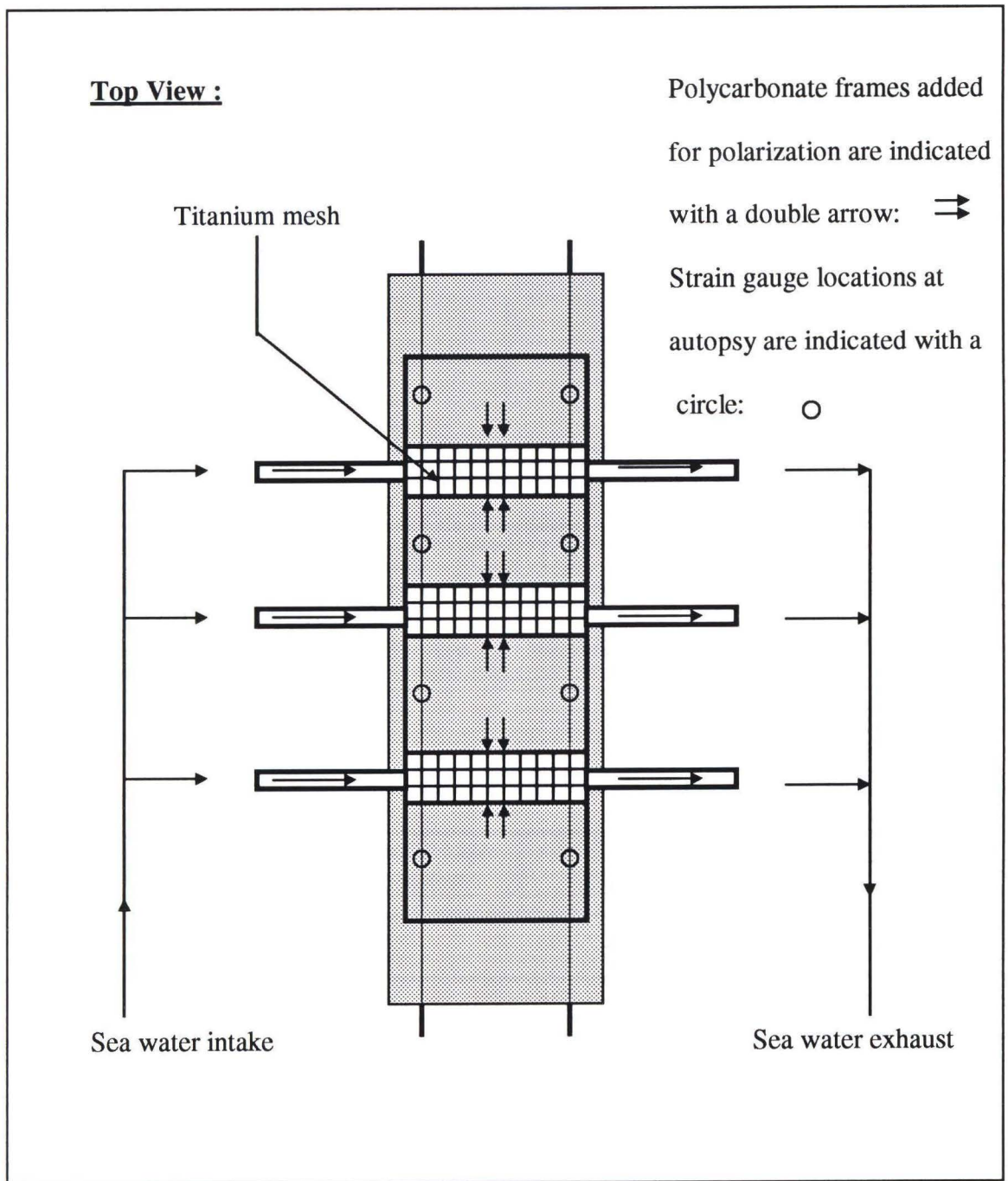


Figure 3-3: Setup for three polarization test areas on a pre-stressed specimen.

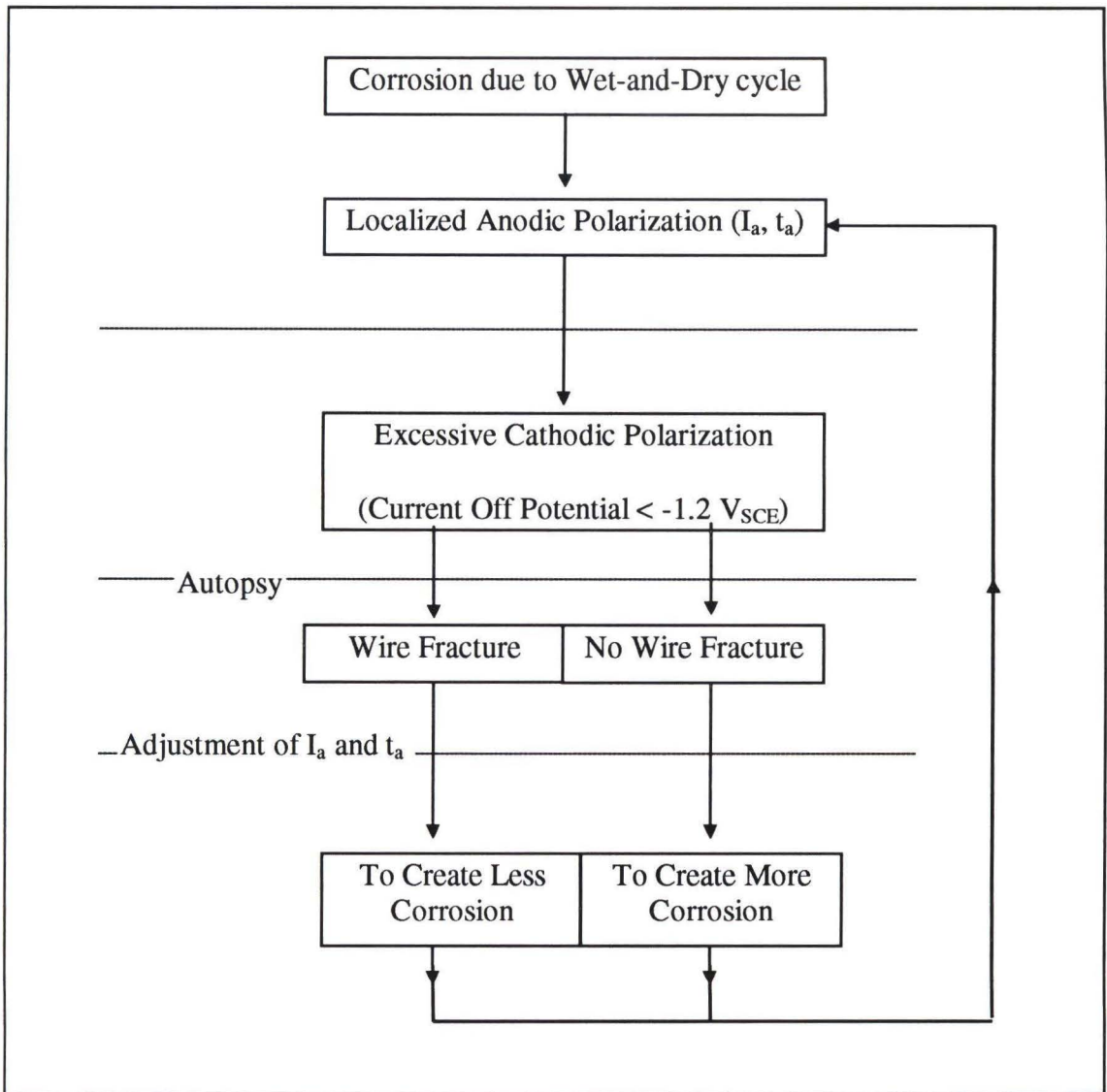


Figure 3-4: Polarization protocol.

In order to cause local free corrosion, two of the concrete specimens (E1 and C3-4) were drilled in the three chloride admixed zones in order to reduce the concrete cover above the tendons to 8 to 13 mm. Then, these drilled zones were locally exposed to wet and dry cycles. The corrosion level was assessed with potential measurements using a saturated gel calomel reference electrode.

3.4 Strain measurements

3.4.1 Purpose and methodology

In order to determine a threshold level of corrosion for hydrogen embrittlement, the pretension in the specimen had to be measured. This involved tendon strain measurements in the central third of the beam and away from anodic polarization ponds before and after autopsy. The measured prestress was assumed to be constant over this central one-third region. This information facilitated determination of the fracture stress of any failed wires and of the residual stress in unfailed ones.

3.4.2 Principle and procedure of strain measurements

Determination of a strain change using strain gauge technology consists of evaluating a strain dependent ohmic resistance relative to a no-strain resistance. Sensitive measurement instrumentation is needed to measure the very small variations of resistance that are involved in this process. A strain indicator is based upon the principle of the Wheatstone bridge, as illustrated in Figure 3.5. Here, the strain gauge is connected as an

unknown resistance R_1 ; and the other known resistances are either internally (R_3) or externally connected (R_2) to the indicator. As measurements had to be taken on the same gauge over an extended period, the strain indicator configuration had to take into account possible temperature changes. As suggested by Hoffmann [29] and confirmed by Joubert on the same specimens employed for the present research [30], thermal drift can be overcome by including in the Wheatstone bridge an unstrained dummy gauge (reference FLA-1-11-1L supplied by T.M.L., Texas Measurements, Inc.) of the same type as the one used for measurement. This was connected as the resistance R_2 in Figure 3.5, and it was mounted upon a bare mild steel plate so that its change in resistance balanced any parasitic deformations of the active gauge. The strain indicated by the active gauge was then considered to reflect the shape change experienced by the member in question. This configuration corresponds to a half bridge connected to the indicator and is called a *compensated quarter bridge*. Before each measurement, the strain indicator (Measurement Group model P3500) was zeroed using the dummy gauge, and then the reading was taken on the tendon gauge.

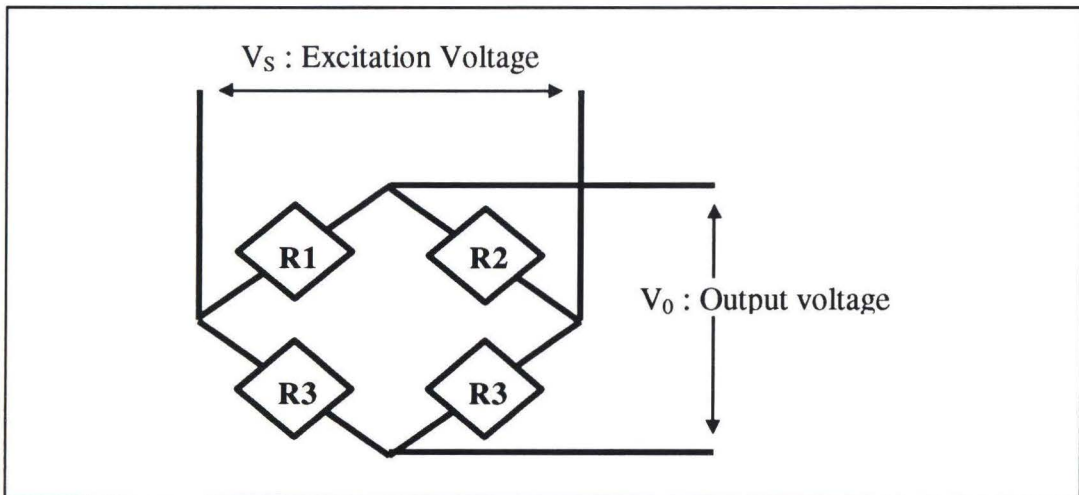


Figure 3-5: Wheatstone bridge circuit.

3.4.3 Strain gauge installation and measurement of tendon strain

In order to compute the strain of the tendon before and any change during the CP phase, the following procedure was developed.

3.4.3.1 Strain gauge installation

First, accesses to the tendon were created on both sides of any local polarization pond in order to mount strain gauges. A grinder was employed for this task, and the access locations were positioned far enough from the polarization pond that the exposed tendon was uncorroded, although they remained within the central one-third of the beam (see section 2.7.1).

Subsequent to grinding, the access was cleaned of any concrete dust; and the steel surface was prepared according to the strain gauge suppliers' instructions [31]. This involved degreasing with a solution of trichloroethylene (reference Measurement Group CSM-1), polishing with coarse then fine paper, if needed, wiping with a gauze sponge dampened successively with degreaser, a water based acidic solution (reference Measurement Group Conditioner A) and a neutralizing solution of water diluted ammonia (reference Measurement Group Neutralizer B) and drying with an air blower. A strain gauge (reference FLA 3 supplied by T.M.L., Texas Measurements, Inc.) was then bonded to a piece of tape (ScotchTM) and evenly coated with glue (M-Bond adhesive resin type AE mixed with 15 % of M-Bond curing agent type AE from T.M.L., Texas Measurements, Inc.). Next, the tape was carefully applied to the tendon such that the gauge was axially aligned on the outer surface of a tendon wire. Finally, a pad of adhesive poster putty wrapped in cellophane laboratory film (ParafilmTM) was positioned on the gauge and maintained under pressure via a u clamp for a minimum of 12 hours. Once the glue was dry, the U clamp was removed and the gauge was usable.

3.4.3.2 Measurement of tendon strain

A strain reading was taken after mounting the gauge, and this was defined as the *initial strain*. During the cathodic polarization phase of some experiments, strain readings were taken on a daily basis. Finally, the specimens were autopsied by breaking them open such that the pre-tension was released. A *final strain reading* was then taken, the strain

difference (difference between *final* and *initial strain*) was computed, and the prestress was computed from this using Hooke's law.

3.5 Tendon analysis

As a part of the specimen autopsy, the extent of corrosion on the individual wires was characterized; and any wire fractures were documented, either visually or by scanning electron microscopy. Also, occurrence of any brittle failure served to define the threshold corrosion level that is acceptable for application of CP.

4 RESULTS AND DISCUSSION

4.1 Evaluation of strain measurements

An experiment was performed to confirm the gauge mounting procedure described in section 3.4.3. This involved mounting a strain gauge upon a single wire, extending the wire to 70 % of its ultimate stress, and then unloading and loading several times. The difference between the measured and computed strains was smaller than 2.2 percent, which led to adoption of the present strain gauge monitoring approach.

The methodology for tendon strain determination presented in section 3.4.3 raised the concern that an inaccurate, abnormally low prestress might be indicated if the strain gauge were mounted on a wire that had corroded in two during the first polarization phase or if the wire had fractured. Consequently, an experiment was performed on beam C3bas3 for the purpose of investigating this. Three access holes were drilled directly above one tendon. The central access (designated as number one) served as a location for cutting individual wires. The two other accesses were located relative to the first such that gauges were attached on the first and sixth wires to be cut. Gauges designated as A and B were located in access number 2, and C and D in access number 3, where access numbers 2 and 3 were two and three tendon twist lengths (32 and 48 cm), respectively, away from number 1. An individual wire was cut on seven consecutive days with strain readings being taken before and after each cutting. Also the prestrain of this region of the

beam was measured at autopsy and equal to $3757 \mu\epsilon$. As illustrated by Figure 4-1, the change in strain from the four gauges did not exceed one percent of the prestrain of the specimen until the last wire was cut; even then, the maximum strain change, obtained with gauge A, was still small (8 percent of the prestrain). Apparently, load was transferred from the cut wire to the remaining ones within the access hole spacing.

Consistent with results for previous research [30] that involved the same instrumentation (gauges, glue, strain indicator and gauge dummy), it was assumed that the maximum systematic strain measurement error was $\pm 100 \mu\epsilon$. Based upon the strain data, it was concluded that the prestress measurement procedure was satisfactory for the tendon load computation and that the accuracy of the procedure should not be affected by wire corrosion or fracture.

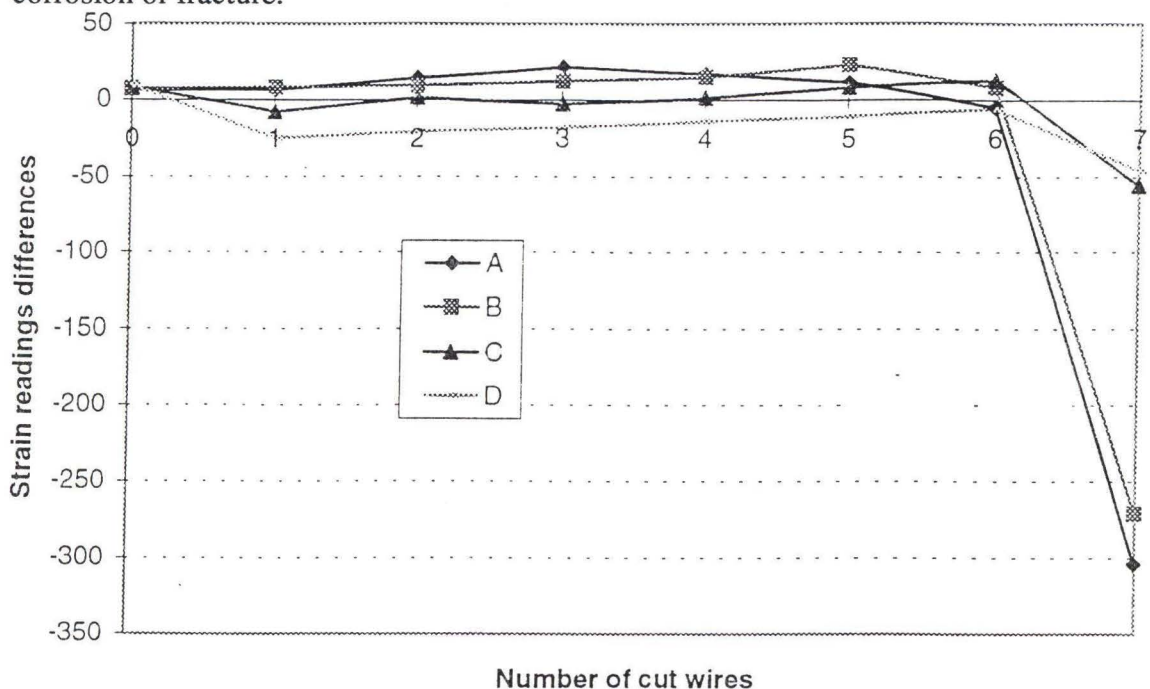


Figure 4-1: Strain reading evolution as a function of the number of wires that had been cut in the central access.

4.2 Level of corrosion

4.2.1 Specimens under anodic polarization

As a preliminary experiment, specimen E4 was equipped with one local pond above only one tendon, and it was subjected to a constant anodic current of 10 mA until the current times time product, $I \times t$, reached 410 mA.days. Considering the tendon surface directly beneath the pond (approximately 31 cm²), the corresponding current density was approximately 320 $\mu\text{A}/\text{cm}^2$. The electrical resistance of the tendon was measured daily in an attempt to detect any wire failure during the anodic and cathodic polarization phases. The autopsy of this specimen revealed that the corrosion level was relatively modest and that no wire failures had occurred. Moreover, during the autopsy, the tendon resistance was continually measured as the specimen was progressively cut into three pieces. It was observed that there was no detectable resistance change until the tendon was fully cut and there was no physical contact between the two tendon ends. Consequently, the resistance measurement was abandoned as a wire fracture detection method; and the $I \times t$ coefficient was subsequently employed as the only corrosion indicator before autopsy.

Subsequently, each tendon of two beams (C3-5 and C3-2) was anodically polarized at four local ponds (three chloride zones plus a zone 50 cm away from an end of the beams) using constant currents from 20 to 90 mA, 640 to 2900 $\mu\text{A}/\text{cm}^2$. After a few days, fine concrete cracks, the occurrence of which could not be correlated with current intensity, developed at several of the ponds; and at two weeks testing at some of the ponds had to

be terminated because of the spreading of cracks. The highest coefficient reached was 1550 mA.days. The autopsy revealed no wire failures.

The next specimen (C3-3) was polarized using only one central pond. A 40 mA (1290 $\mu\text{A}/\text{cm}^2$) constant anodic current was applied until $I \times t$ reached 1760 mA.days. A crack developed which required frequent patching. The autopsy showed that no wire failures occurred.

The next specimen (C3-11) was tested also with a single pond, but the anodic current was 2 mA (64 $\mu\text{A}/\text{cm}^2$) for the first day and was then increased by 2 mA daily until a level of 46 mA (23rd day) corresponding approximately to a current density of 1480 $\mu\text{A}/\text{cm}^2$ was reached. The current was then maintained constant until the end of the anodic polarization phase, at which time $I \times t$ had reached 2120 mA.days. In this case the amount of concrete cracking was less than in the previous beams. The autopsy revealed one broken wire on the South tendon as shown in Figure 4.2. The minimum measured cross section for each wire of this tendon and the fracture surface area for the broken wire are listed in Table 4-1. The fact that one of the wires was fractured indicated that either the local cross section was reduced to the extent that its ultimate strength was exceeded or the wire was hydrogen embrittled (alternately, these two factors combined could have been the cause). Because the fracture surface was corroded, it was concluded that the breakage occurred during the anodic rather than cathodic polarization phase of the test. The analysis was not extended to the North tendon as all its wires remained unbroken and the cross section reduction due to corrosion was minor.

Specimen C3bas4 underwent the same polarization plan as specimen C3-11 to an $I \times t$ value of 2720 mA.days. The resultant corrosion level was anticipated to represent a more severe corrosion situation than for specimen C3-11 ($I \times t$ value of 2120); however, no wire failures were disclosed. Table 4-2 lists the minimum remaining cross section for each wire for this case.

The visual appearance of specimen C3bas4 indicated that once a certain level of anodic charge transfer was reached, corrosion tended to spread rather than remain concentrated in a local zone. Consequently, it was decided to test the next several specimens to a higher $I \times t$ value to increase the chances of inducing wire fractures. Thus, specimens C3-9, E10 and E9 were anodically polarized with increasing currents in one central local pond to $I \times t$ values of 3790, 4300, and 4430 mA.days, respectively. The minimum wire cross sections that were measured upon autopsy are listed in Table 4-3. This shows that relatively high levels of corrosion were obtained. The length along the tendon of most intense corrosion (locations of minimum wire cross section) was always smaller than the twist length (16 cm). In spite of the relatively high number of wires that corroded in two, no fractures were detected; and the remaining wires bore the tendon load. (Note: The possibility exists that fractures occurred during the anodic polarization phase of the tests and that subsequent corrosion precluded these from being identified as such).

Table 4-1: Minimum remaining cross section of tendon wires in specimen C3-11.

Wire Numbers *	Minimum wire cross section, mm ²
1	2.8 **
2	6.1
3	6.5
4	5.8
5	7.5
6	5.7
7	11.4
Tendon	43

* Side wires are numbered from 1 to 6 and number 7 is the central wire.

** Based upon scanning electron microscopic observation of the fracture surface area.

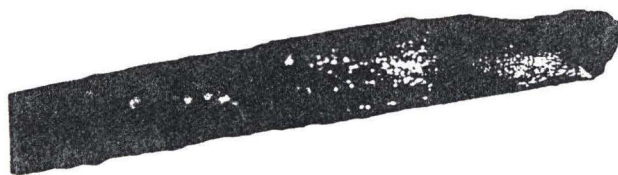


Figure 4-2: Photograph of the broken wire from specimen C3-11.

Table 4-2: Minimum remaining cross section of tendon wires in specimen C3bas4.

Wire Numbers *	Minimum wire cross sections, mm ²	
	C3bas4 North	C3bas4 South
1	7.7	7.5
2	7.1	4.4
3	6.1	6.2
4	5.6	4.5
5	7.1	6.8
6	6.4	6.2
7	11.7	11.7
Tendon	51.7	47.3

* Side wires are numbered from 1 to 6 and number 7 is the central wire.

Table 4-3: Minimum remaining cross section of tendon wires in specimens C3-9, E 10 and E 9.

Wire number	Minimum wire cross sections, mm ²					
	C3-9 North	C3-9 South	E 10 North	E 10 South	E 9 South	E 9 North
1	CC	CC	CC	1.1	CC	CC
2	CC	CC	CC	3.0	CC	CC
3	4.7	CC	CC	.8	CC	CC
4	4.3	CC	CC	1.6	CC	CC
5	CC	2.8	CC	6.1	CC	CC
6	4.6	2.5	7.2	4.1	CC	CC
7	10.9	10.5	9.7	10.2	5.7	9.1
Tendon	24.5	15.8	16.9	26.9	5.7	9.1

CC indicates the wires that had corroded in two.

4.2.2 *Drilled specimens under wet and dry cycle exposure*

The two drilled specimens (E1 and C3-4) underwent wet and dry cycles for more than one year; but as tendon potentials did not indicate significant corrosion, the experiment upon other beams was modified. For specimens E 5, E 6, C 3-6 and C 3-1, four 40 mm. diameter holes were drilled similar to those for specimens E1 and C3-4 (see section 3.3) except that the concrete cover above the steel at the base of the hole varied from 0 to 8.5 mm. In the case of zero cover the drill bit contacted and exposed a local region of the tendon. These specimens plus specimen C3-4 were anodically polarized with an increasing current in local ponds above the holes and then were subjected to excessive CP. For each tendon, the two polarization zones were referred to as East (side) and West (center). The $I \times t$ values and the minimum wires cross sections that resulted are summarized in Table 4-4.

Table 4-4: Ixt values and minimum remaining cross sections for specimens C 3-4, E 5, E 6, C 3-6 and C 3-1.

Beam		Ixt mA.day	Minimum wire cross sections, mm ²							Tendon area, mm ²
			Wire #1	Wire #2	Wire #3	Wire #4	Wire #5	Wire #6	Wire #7	
C3-4	NW	3402.4	CC	CC	CC	CC	CC	3.8	10.8	14.6
	SW	3402.4	CC	CC	5.7	4.1	4.0	4.6	10.9	29.4
E5	NE	730.2	CC	5.5	10.4	10.4	10.4	9.1	10.9	56.7
	NW	643.9	CC	CC	CC	8.3	5.9	9.3	CC	23.5
	SE	730.2	CC	CC	5.2	9.7	10.4	4.1	10.7	40.1
	SW	643.9	7.4	4.8	9.1	9.1	9.0	8.4	10.9	58.7
E6	NE	892.6	CC	CC	CC	CC	CC	4.2	CC	4.2
	NW	793.9	CC	CC	3.7	5.6	3.8	3.2	2.3	18.6
	SE	892.6	CC	CC	8.4	10.4	10.4	8.7	9.8	47.7
	SW	793.9	CC	CC	CC	5.6*	8.5	10.1	CC	18.6
C3-6	NE	827.2	CC	CC	CC	8.0	9.5	10.4	2.8	30.7
	NW	770.1	CC	CC	8.8	10.2	8.4	6.4	10.3	44.1
	SE	827.2	CC	CC	CC	CC	4.9*	8.1	CC	8.1
	SW	770.1	CC	CC	CC	2.8*	8.2	2.9	CC	11.1
C3-1	NE	1947.1	CC	CC	2.2	2.2	2.3	1.7	8.9	17.3
	NW	2256.9	CC	CC	CC	CC	CC	CC	CC	0.0
	SE	2143.6	CC	1.1	7.6	2.6	1.5	2.0	9.8	24.6
	SW	2256.9	4.0	6.8	5.3	5.9	4.7	3.9	10.5	41.1

CC indicates wires that corroded in two.

* indicates fracture section areas.

Because of concrete cracks that developed during the anodic polarization phase, only the central zone of specimen C3-4 underwent both anodic and cathodic polarization. Based upon the minimum tendon cross section (sum of minimum wires cross sections, see last column of the table), it is apparent that different levels of corrosion were reached upon the tendons and the cross section reductions did not correlate with the $I \times t$ values. This apparently resulted because of differences in local cover at the base of the drilled holes and of the occurrence of concrete cracking. Thus, when the sea water had direct access to the steel due to either of these causes, corrosion was intense; and the tendon was consumed locally with a cup shape morphology. Figure 4.3 shows this particular feature for specimen E6 at the NE pond, where the tendon was corroded to the point where only a portion of one wire was left. In spite of the high levels of corrosion that were reached, only specimens E6 and C3-6 exhibited a fracture due to excessive CP. These fractures are shown in Figure 4.4 for specimen E6 and Figure 4.5 and 4.6 for specimen C3-6.



Figure 4-3: Cup shape corrosion at the NE pond for beam E6.

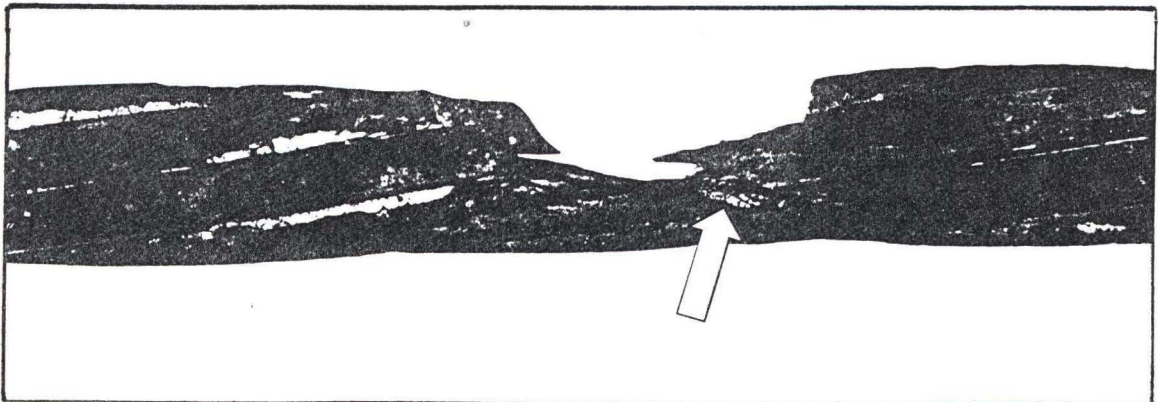


Figure 4-4: Brittle fracture of tendon wire of specimen E6 at the SW pond.

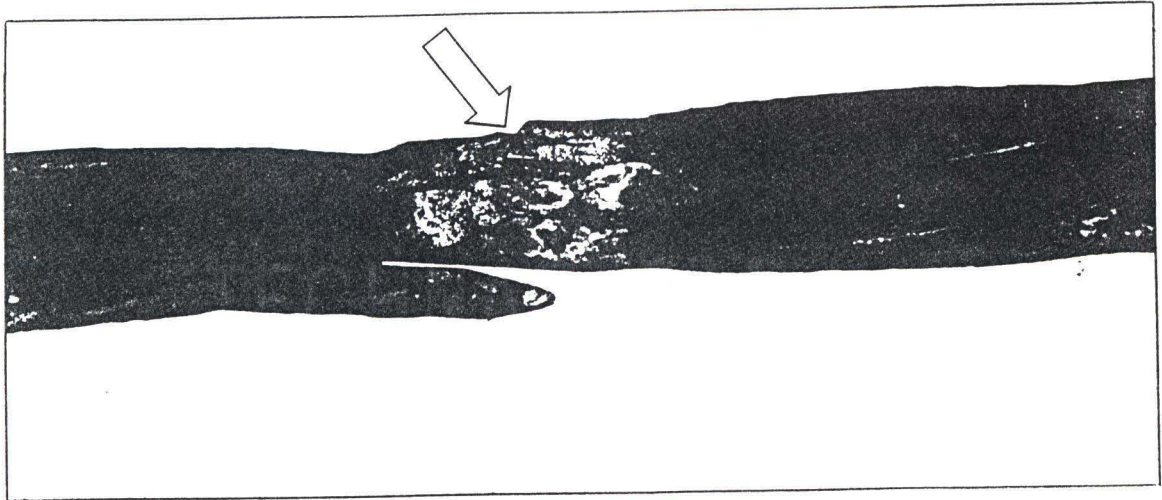


Figure 4-5: Brittle fracture of tendon wire of specimen C3-6 at the SW pond.

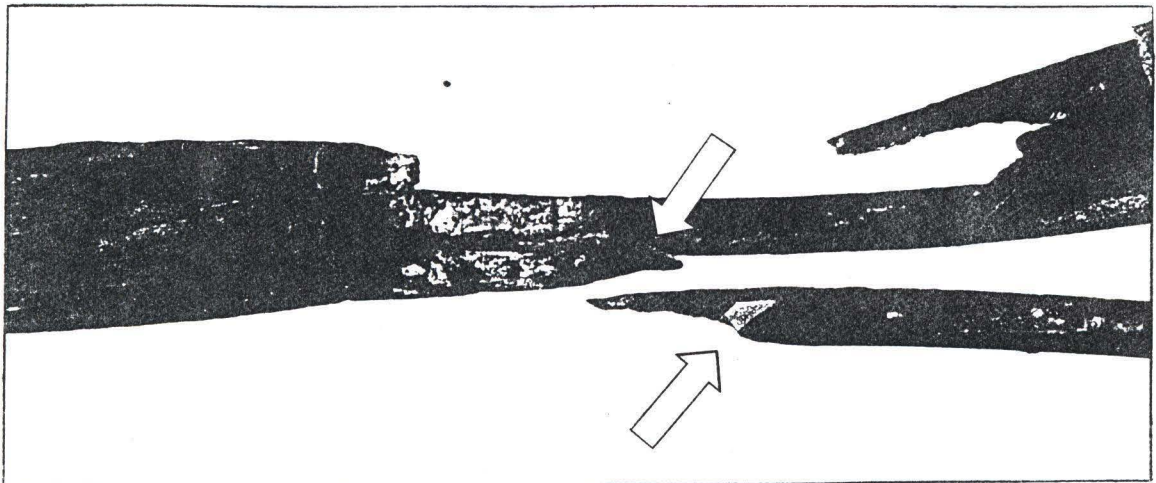


Figure 4-6: Brittle failure of tendon wire of specimen C3-6 at the SE pond.

4.3 Shape of corrosion pits

All the specimens that were not drilled before polarization (see section 3.3) generally exhibited similar corrosion features. When the depth of corrosion was smaller than approximately one-third of the wire diameter, the depth to length ratio (d/l) was typically about one third; but when depth was higher than one third of the wire diameter, the corrosion was flatter; and d/l rarely exceeded 6×10^{-2} . A parallel study [32], which was also performed on Grade 270 tendon wires, showed that this elongated corrosion morphology was related to the cold drawn microstructure. The experimental setup that resulted in the cup shaped corrosion also led to corrosion morphology that was elongated in the wire axis direction, but d/l was higher than for the specimens that had not been drilled in the polarization zones. Apparently, corrosion morphology in the drilled specimen case was affected by IR drop which constricted the current to near the base of the holes. For specimens that were not drilled, the central wire was generally the last one to corrode in two, since it only became exposed to the electrolyte after the outer wire(s) had corroded; however, the experimental set-up involving holes drilled to near the tendon caused corrosion to occur first on the top and central wires before the bottom. Moreover, when side wires bore all the tendon load, as in the latter case, they also had to support an extra shear stress component compared to when only the central wire, which is straight, remained. Consequently, drilled specimens underwent a more severe stress than is expected for tendons in actual structures; and so results for these are likely to have been conservative.

4.4 Strain measurements

The strain measurement procedure developed by Joubert [30] was employed for the first seven polarized beams (E4, E1, C3-4, C3-5, C3-2, C3-3, C3-8); however, this was found not to be reliable. Consequently, strain data are not reported for these specimens. The technique described in section 3.4.3 was developed for the next specimens. However, the experience gained with the first seven specimens aided development of this procedure and determination of the requisite level of corrosion as reflected by the $I \times t$ parameter. Also apparent is that the levels of corrosion that were reached were not sufficient to cause hydrogen embrittlement upon application of excessive CP.

The strain reading differences that were obtained are summarized in Table 4-5, and these are assumed to be a measure of the prestrain that exists in the respective tendons. The various sites where strain was measured are designated for both (North and South) tendons as C if only one gauge was used per tendon in the center of the beam, by W and E (West and East) if two gauges were employed per tendon, or by W, C and E if three were used per tendon. An X indicates that the measurement attempt failed. Data labeled (B) or (U) indicate the gauge turned out to have been mounted on either a broken or an unbroken side wire, respectively; but for most specimens this information was not acquired during autopsy. For specimen E9 at the NW pond, the strain presented as less than $1195 \mu\epsilon$ corresponds to an intermediate reading since the gauge failed before a final reading could be acquired.

The strain reading obtained for the NC pond of specimen C3-1 ($-2028 \mu\epsilon$) was slightly above the average of all the specimens ($-1912 \mu\epsilon$). However, this was measured less than

22 cm away from a location where the entire tendon had corroded in two. This reading of $-2028 \mu\epsilon$ is comparable to the one that was obtained on the other tendon of this specimen at the SC pond ($-1939 \mu\epsilon$), indicating the development length that corresponded to the tendon having corroded in two was shorter than 22 cm. The experiment which involved specimen C3bas3 (see section 4.1) indicated that about 90 percent of the prestress was retained in 32 cm (two tendon twist lengths) in a case where the prestress was 777 MPa. Results from these two experiments indicate that the prestress was developed on a smaller length than the computed development length (1m).

For specimens E9 and E10, strain gauges were installed before anodic polarization. The strain was checked daily; and the results are given in Figure 4-7 for specimen E9 and Figure 4.8 for specimen E10.

Table 4-5: Prestrain measurement results.

Specimens	Prestress strain, $\mu\epsilon$					
	NW	NC	NE	SW	SC	SE
E2		-493			-2581	
C3-11	X		-3426	-3613		-3469
C3bas4	-114		-2256	-2191		-2046
C3-9	-3063		-2726	+24		-1819
E10	X		X	-3145		-2441
E9	<-1195		-953	-1433		X
C3-4	-324 (B)		-1653 _(lastU)	X		-254 (U)
E5	-1196	-3628	-3031	-1215	-2119	-1133
E6	-2144	-1819	9	-3620	-2772	-861
C3-6	-2318	-387	-1741	-1569	-3214	-1110
C3-1	X	-2028	-1151	-58	-1939	X
E1	-1164	-671	-657		-1441	
C3bas3		-3854		-2518	-3757	-2563

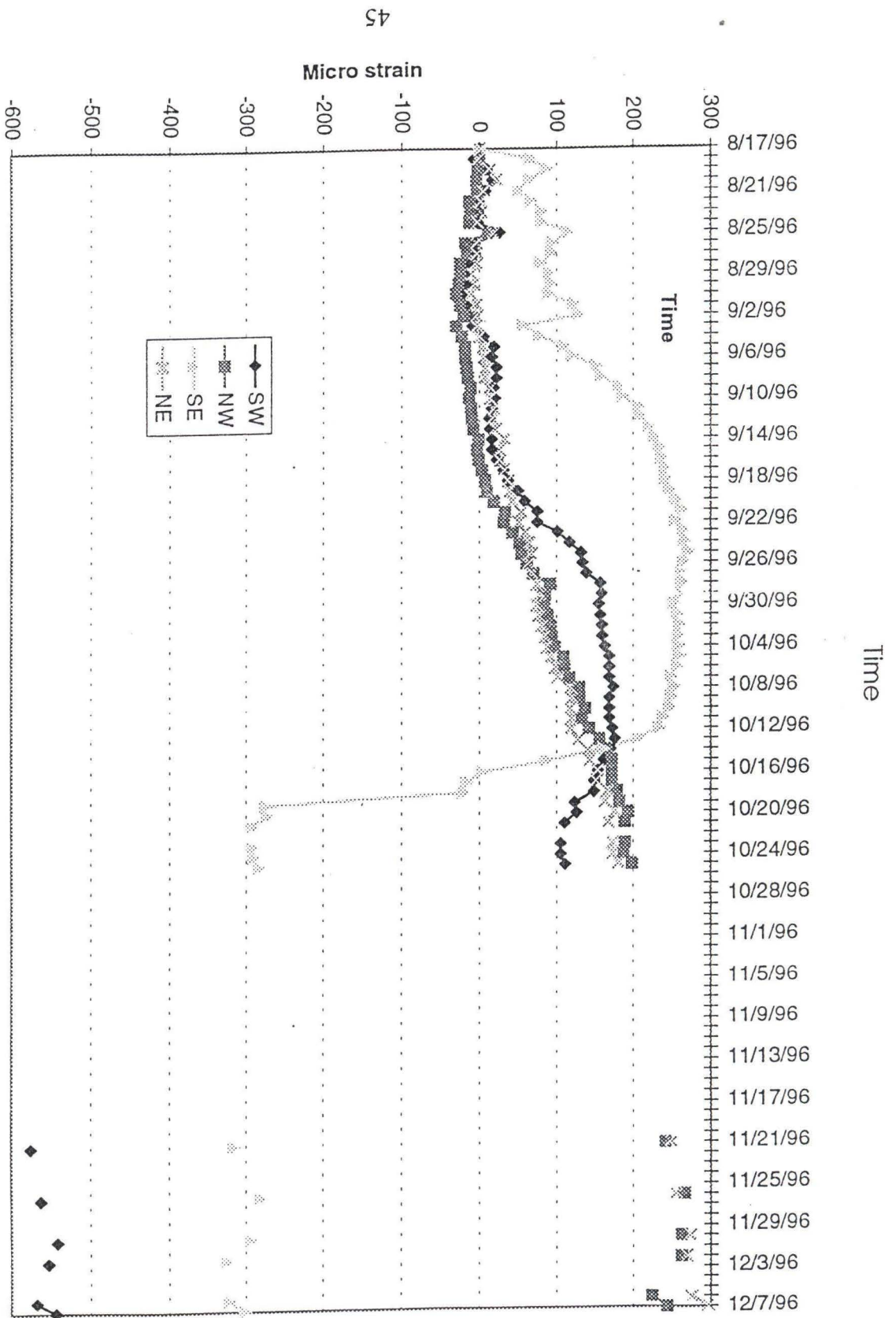


Figure 4.7: Strain evolution during polarization of E9.

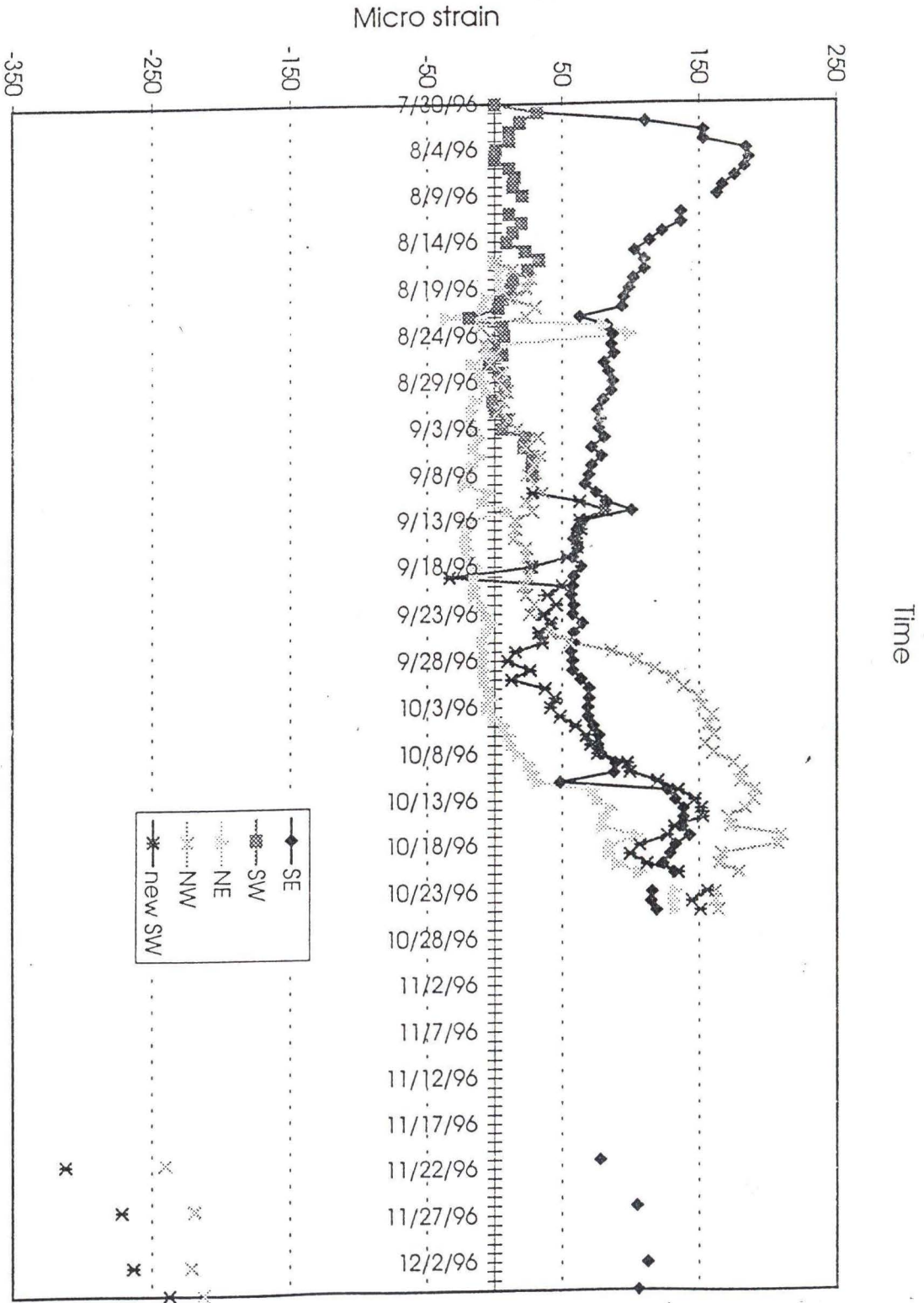


Figure 4-8: Strain evolution during polarization of E10.

It is apparent that, for these two beams, the variations in the measured strain with time were generally the same for each of the four gauges. One exception was the gauge labeled SE on specimen E9. This gauge was changed a few days before autopsy because its readings were unstable compared to the others. However, the replacement gauge indicated no strain change as this specimen was autopsied, meaning either that the tendon was unstressed in that zone or the new gauge was faulty.

It must be noted that these beams were anodically polarized for three (for E9) and almost four months (for E10) without pre-drilling the surface. As a consequence, the corroded zones were about twice as long as for specimens which had holes drilled in the concrete to near the steel depth (40 rather than 20 cm). The micro-strain did not vary more than 300 units during the anodic polarization, which is considered small compared to the average prestrain (-1912 $\mu\epsilon$). Moreover, the gauge setup involved atmospheric exposure of tendon areas where gauges were glued. These areas exhibited some corrosion, and this presented a risk of gauge failure. Also, any grinding before CP was a potential risk for prestress loss. It was decided from this not to place gauges on subsequent specimens before the end of the CP phase.

Daily strain readings on E9 and E10 were stopped after the first two to three months of anodic polarization. Then, readings were taken again during CP (beginning 11/21/96). Comparison of the data obtained at the beginning of anodic polarization with those acquired during CP indicated general correspondence between the two for the NE and NW locations of specimen E9 and SE location of specimen E10. However, some data show a negative mismatch of 450 to 700 $\mu\epsilon$ in spite of the finding that these exhibiting

normal behavior during autopsy (SW gauge for both specimens). This can not be attributed to a difference between gauges mounted on broken and unbroken wire, because, as described in Table 4-3, all the side wires of specimen E9 severed during anodic polarization. However, these two specimens had the highest $I \times t$ values; and their tendon cross section area was reduced over a relatively long length (approximately 40 cm). Consequently, the steel-concrete bond may have been irregularly reduced and the six severed side wires may have released some prestress at the location of gauges E9 SE and SW and E10 NW and SW.

4.5 Analysis of specimen pretension

According to the design and fabrication practice of the specimens, each uncorroded tendon (74 mm^2 cross section area) was pre-loaded to 104 kN (23,300 lb.) or 75 % of ultimate. However, as indicated in Table 4-5, the highest prestrain value recorded (SC pond of specimen C3bas3) was $3757 \mu\epsilon$ which corresponds to less than 42 % of ultimate. The average pre-strain was $1912 \mu\epsilon$ (less than 22 % of ultimate), and the standard deviation was $1113 \mu\epsilon$. Gauges mounted upon tendons of the unpolarized beams (E1 and C3bas3) exhibited an average reading of $2080 \mu\epsilon$ which is 10 percent higher than the average for polarized specimens ($1891 \mu\epsilon$). Consequently, the low strain readings can not be attributed to stress release due to the polarization procedure. It is concluded that prestress in the present specimens was unexpectedly low, and that this may have been a contributing factor to the finding that only a few wire fractures were detected.

4.6 Determination of the stress level in a corroded wire

It can be reasoned that tendon load should remain the same as corrosion develops until a corrosion limit is reached, at which point the ultimate stress is exceeded and failure occurs. However, such a process is complicated by the fact that the tendon may extend locally as its cross section is consumed and, hence, release prestress. In order to compute the stress level at corroded wire locations and define this limit, a model was developed which projects load and stress evolution in the individual wires as corrosion progresses.

4.6.1 Computation of the tendon load

In an uncorroded zone of a seven-wire tendon, the net load is given by

$$P_t = \sum_{1to7} (P_i) = \sum_{1to7} (\sigma_i \times A_i) = \sum_{1to7} ((E \times \epsilon_i) \times A_i) \quad 1)$$

where P_t = Total load carried by the tendon.

P_i = Partial load in i th wire.

σ_i = Stress in i th wire for the cross section of interest.

A_i = Cross section of i th wire in the cross section of interest.

E = Elastic modulus of the steel.

ϵ_i = Strain of the i th wire in the cross section of interest.

The experimental procedure involved strain measurement of a side wire. Because these are twisted around the central wire and are longer, strain in the two is not equal. The difference in strains was computed for stresses up to ultimate as described in the appendix. This indicated that the difference was smaller than the error in the strain readings (see section 4.1); and so, in an uncorroded zone of a tendon, the measured strain

upon a spiraled wire was assumed to apply also to the central wire. On this basis, equation 1) may be rewritten as

$$P_t = E \times \epsilon_{side} \sum_{1to7} (A_i) \text{ or } P_t = E \times \epsilon_{side} (6 A_s + A_c), \quad 2)$$

where A_s and A_c represent the cross section area of uncorroded side and central wires, respectively. Consequently, stress was assumed to be the same in each of the seven wires of an uncorroded tendon.

4.6.2 Theoretical model

It was observed after autopsy of the specimens that most of the severed wires were heavily corroded. This suggests that these fractured during the anodic polarization phase of the tests once wire cross section was sufficiently reduced and that corrosion continued afterwards. A few wires exhibited fractures without corrosion products on the fracture face which was considered indicative of failure during cathodic polarization (hydrogen embrittlement). These observations were used to develop a model that addresses load and stress state changes as an individual wire corrodes and defines those conditions that lead to failure.

As long as no generalized tendon yielding occurs, it is assumed that the load is constant along a tendon whatever the level of corrosion and the number of broken wires in the investigated cross section. When a tendon is uncorroded, each of the seven wires has the same displacement and undergoes the same stress, as discussed above. If corrosion develops uniformly on a local zone of a wire, its strain increases due to the reduction of cross section area, assuming that the wire cannot contract since it is constrained by its

bond to the concrete beyond the corroded zone. However, the tendon load remains constant, as indicated by the experimental results presented in section 4.1. which showed that at a given distance away from the corrosion zone (slightly more than 3 tendon twist lengths), the stress state was conserved and the local strain was unchanged as individual wires were sequentially cut. This situation is illustrated schematically in Figure 4-9.

If the bond is maintained beyond the corroded region (BC in Figure 4-9), which represents an extreme situation where corrosion does not affect wire strain in the uncorroded cross section beyond BC, then the strain remains the same for the seven wires outside the corroded region and is equally increased in the seven wires in the region where the cross section of the single wire is reduced ($\delta' > \delta$ in region BC). The elastic stress (σ) in a wire of constant cross section is given by $\sigma = E \times \epsilon$, where E is the modulus of elasticity and ϵ the strain. As wires have the same modulus of elasticity and the assumption is the seven wires undergo the same strain in the corroded region BC, it can be deduced that within BC stress is equal in all wires and larger than before corrosion. The local increase in strain occurs in association with a load transfer from the corroding wire to the others. If the tendon does not fracture as either the first wire fails or corrodes in two, the process can repeat itself as a second wire corrodes, and so on. When the stress in any wire within BC reaches the yield stress, further increments in stress yield plastic strain changes that may be accompanied by load release of the tendon within BC and a prestress decrease in concrete surrounding the corroded zone.

A second extreme situation is considered where corrosion in the region BC causes a bond loss over a length AD where $AD \gg BC$. As long as general yielding of the tendon does

not occur, the beam load is assumed to be constant. At any time, the length dimensional components in the corroding wire (see Figure 4-10) conform to the relationship

$$L_{AD} = L_{AB} + L_{BC} + L_{CD}, \quad 1)$$

where

L_{AD} = length of the region AD in the 7 wires;

L_{AB} (or L_{CD}) = length of the region AB (or region CD) in the corroding wire; and

L_{BC} = length of the region BC in the corroding wire;

As the cross section area of the corroding wire in region BC reduces from A_0 to A , its strain increases by

$$\Delta \epsilon_{BC} = P_i / ((A - A_0) \times E) = (\delta' - \delta) / \delta,$$

where the corresponding length increase is $(\delta' - \delta)$. Since $L_{BC} \ll L_{AD}$, this extension of BC is balanced by a decrease of the strain in the uncorroded regions of this wire (AB and CD) by an amount equal to $(\delta' - \delta) / (L_{AB} + L_{CD}) = (\delta' - \delta) / (L_{AD} - L_{BC}) \cong (\delta' - \delta) / (L_{AD})$ which is negligible. Consequently, load in the corroding wire remains constant and is considered equal* to that in the uncorroded wires until the corroding wire fractures. Thus, the zone of highest stress is localized to within the corroded section. When this stress reaches the yield stress, further corrosion leads to plastic strain and ultimately to fracture of the wire. As this occurs, load in this wire is transferred to the uncorroded wires. The process can then repeat itself until fracture of a corroding wire results in a stress in the remaining uncorroded wires which is above the yield stress. Then, any further cross section area reduction causes cross section plastic deformation which can ultimately lead to failure of the whole tendon.

** In the present seven wires tendons, the cross section area for uncorroded side and central wires is equal to 10.4 and 11.4 mm², respectively. Consequently, in an uncorroded tendon, assuming that the strain is the same in the different wires is equivalent to assuming an equal stress too; but the cross section areas are different so such an assumption is equivalent to the assumption of a higher load in the central wire. However, assuming that the partial loads are equal in an uncorroded tendon is equivalent to over estimating of 1.4 % the initial load in side wires, which is considered negligible.*

These two corrosion models are termed “equal stress” and “equal load”, respectively, because of the condition that results in wires. They represent two extremes in which corrosion of a localized area of a tendon alters the strain state of the tendon either in the corroded cross section only (complete bond retention beyond the corroded zone) or in a zone that includes an uncorroded region much longer than that of the corroding region (bond loss beyond the corroded zone). In the first case corrosion leads to a progressive load transfer from the corroding to uncorroded wires, whereas in the second load transfer only occurs at fracture of a corroding wire.

In specimens E9 and E10, daily strain measurements (see Figures 4-7 and 4-8) taken approximately 30 cm away from the center of the polarization pond showed some change with time which means that the equal stress model was not fully applicable. On the other hand, the equal load model indicates that strain should have increased in increments as individual wires failed; but this was not the case either as strain changes seemed continuous. This suggests that in actuality the stress state changes which accompanied this corrosion were intermediate between these two extremes. In other words, some load

transfer from the wire of smallest cross section to the others occurred but not to the point where this wire corroded in two without failing.

The experimental data in section 4.1. indicated that bond was retained within slightly more than three twists lengths from a location where a tendon had fractured or corroded in two. For the present experiments corrosion was such that the minimum cross section area of the various wires was within a two tendon twist lengths spacing, which seems to preclude much bond retention in this zone. It must be noted too that in actual prestressed concrete structures, pretension is generally transferred to the concrete by a matrix of tendons whose stress fields overlap. Consequently, L_{AD} for one tendon may be minimal due to the compressive action on the concrete by adjacent tendons.

It can be reasoned that in the early stages of corrosion when attack is localized, the concrete-steel bond is affected over a distance which is large in comparison to that of the corroded zone; and the equal load theory may be appropriate. On the other hand, when corrosion becomes more developed and the zone of reduced cross section spreads, the difference in length between the two zones reduces. In this case, the stress state should tend to transition to the constant stress case.

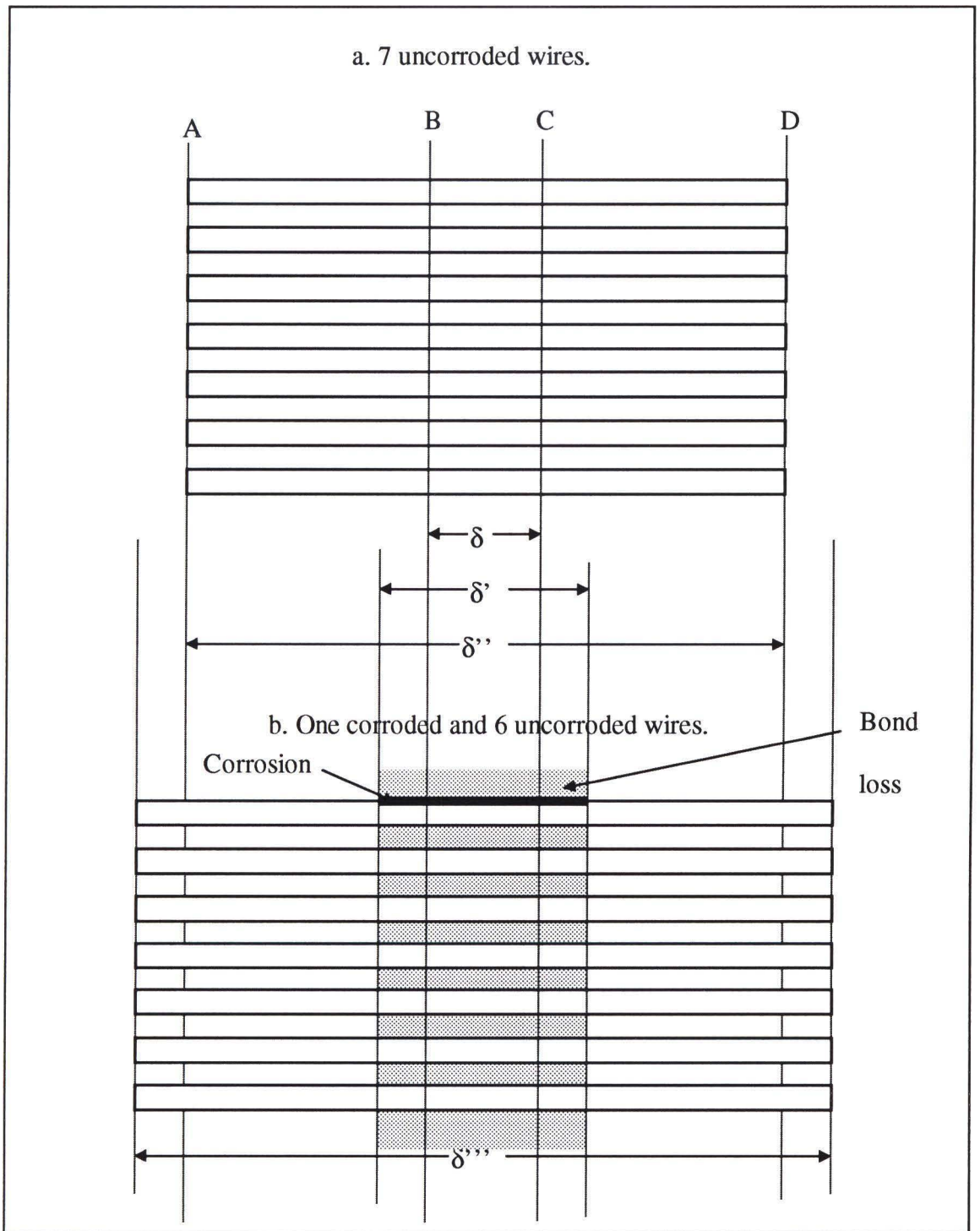


Figure 4-9: Corrosion evolution with equal stress between wires in the corroded region.

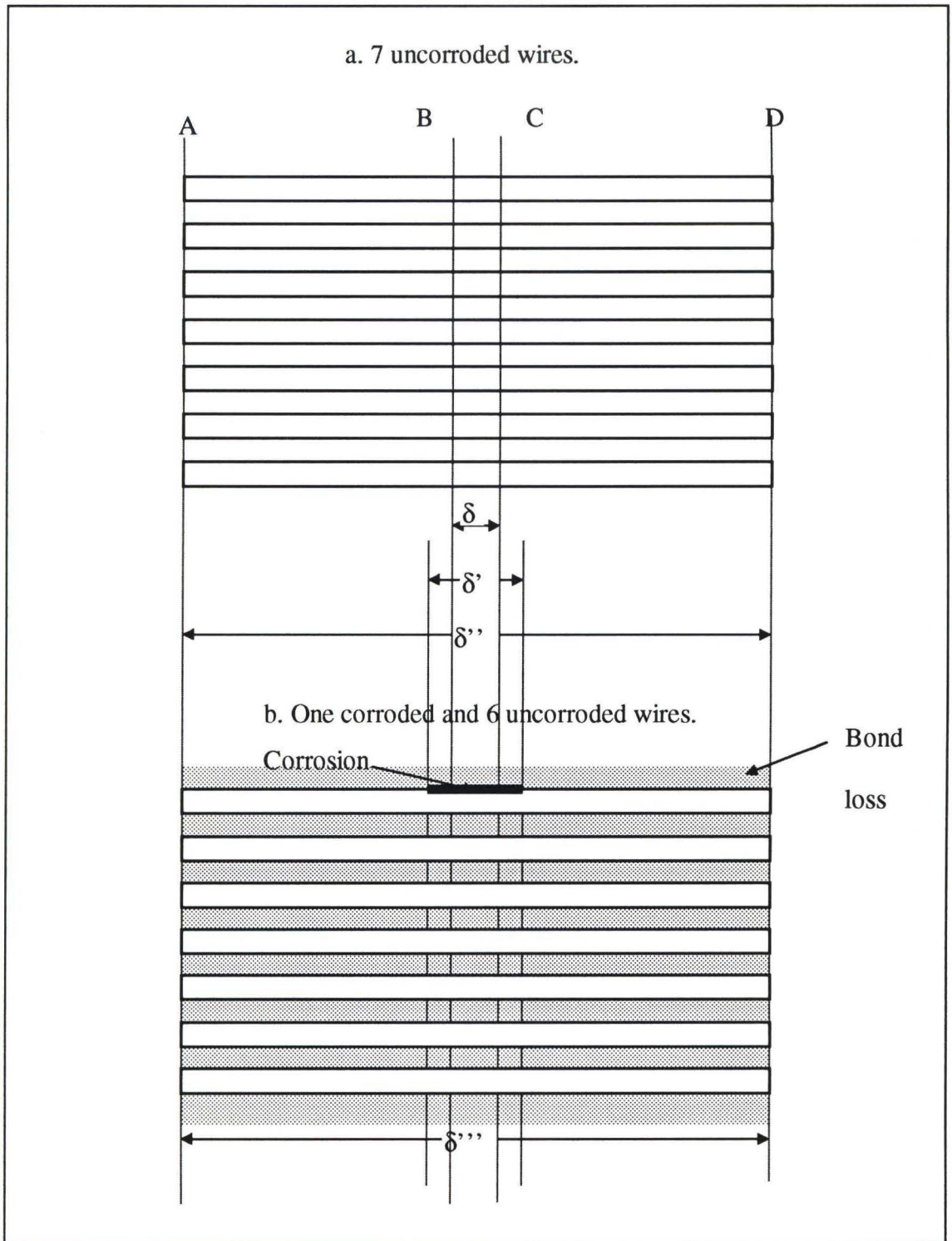


Figure 4-10: Corrosion evolution with equal partial load in unsevered wires.

4.6.3 Evaluation of data

The strain readings and level of corrosion data collected from the specimens were used to evaluate the theoretical models. As the importance of load transfer from the wire of smallest cross section area to the others could not be evaluated for intermediate levels of corrosion, the stress was computed for each specimen using the equal load approach in order to define the fit of this model. The tendon load was determined from the strain measurements. These computations were performed with the strain reading obtained on each side of the corroded region.

4.6.3.1 Calculations for specimen E5.

Pond NW:

- Using $\epsilon_{\text{maximum}} = 3,628 \mu\epsilon$ (Table 4-5) and $E = 207 \text{ GPa}$,

$\sigma = \epsilon \times E = 750 \text{ MPa}$ (108.8 ksi) and $P_{\text{total}} = 55,531 \text{ N}$ in an uncorroded section.

$P_i = P_{\text{total}} / 3$ (Table 4-4) = 18,510 N leading to $\sigma_{\text{most corroded}} (\sigma_{\text{mc}}) = 3,158 \text{ MPa}$ (458 ksi) in the wire of smallest section area (Table 4-4).

- Using $\epsilon_{\text{minimum}} = 1196 \mu\epsilon$

$\sigma = 248 \text{ MPa}$ (36 ksi) and $P_{\text{tot.}} = 18,306 \text{ N}$ in an uncorroded section.

It leads to $\sigma_{\text{mc}} = 1041 \text{ MPa}$ (151 ksi).

Pond NE:

- Using $\epsilon_{\text{maximum}} = 3,628 \mu\epsilon$

$\sigma = 750 \text{ MPa}$ (108.8 ksi) and $P_{\text{tot.}} = 55,531 \text{ N}$ in an uncorroded section.

$P_i = P_{tot}/6 = 9,255 \text{ N}$ leading to $\sigma_{mc} = 1,675 \text{ MPa}$ (243 ksi) in the wire of smallest section area.

- Using $\epsilon_{minimum} = 3,031 \mu\epsilon$

$\sigma = 627 \text{ MPa}$ (90.9 ksi) and $P_{tot.} = 46,394 \text{ N}$ in an uncorroded section.

$P_i = P_{tot.}/6 = 7,732 \text{ N}$ leading to $\sigma_{mc} = 1401 \text{ MPa}$ (203.16 ksi) in the wire of smallest section area.

Pond SW:

- Using $\epsilon_{maximum} = 2119 \mu\epsilon$

$\sigma = 438 \text{ MPa}$ (63.6 ksi) and $P_{tot.} = 32,434 \text{ N}$ in an uncorroded section.

This leads to $\sigma_{mc} = 965 \text{ MPa}$ (140 ksi) in the wire of smallest section area.

- Using $\epsilon_{minimum} = 1215 \mu\epsilon$

$\sigma = 251 \text{ MPa}$ (36.4 ksi) and $P_{tot.} = 18,597 \text{ N}$ in an uncorroded section.

This leads to $\sigma_{mc} = 556 \text{ MPa}$ (80.6 ksi) in the wire of smallest section area.

Pond SE:

- Using $\epsilon_{maximum} = 2119 \mu\epsilon$

$\sigma = 438 \text{ MPa}$ (63.6 ksi) and $P_{tot.} = 32,434 \text{ N}$ in an uncorroded section.

This leads to $\sigma_{mc} = 1,599 \text{ MPa}$ (232ksi) in the wire of smallest section area.

- Using $\epsilon_{minimum} = 1133 \mu\epsilon$

$\sigma = 234 \text{ MPa}$ (34.0 ksi) and $P_{tot.} = 17,342 \text{ N}$ in an uncorroded section.

This leads to $\sigma_{mc} = 856 \text{ MPa}$ (124 ksi) in the wire of smallest section area.

4.6.3.2 Application to all the specimens

The same computations were performed for each of the specimens. The results are summarized in Table 4-6 for computations based on ϵ_{\max} and in Table 4-7 for computations based on ϵ_{\min} .

Table 4-6: Summary of the stress computations based on maximum strain readings.

Specimens number and pond designation	Strain in $\mu\epsilon$.	Stress ksi / MPa	Number of unbroken wires
E 5 NW	$\epsilon_{\max} = -3628$	458 / 3,158	3
NE	$\epsilon_{\max} = -3628$	243 / 1,675	6
SW	$\epsilon_{\max} = -2119$	141 / 972	7
SE	$\epsilon_{\max} = -2119$	232 / 1,600	5
E 10 S	$\epsilon_{\max} = -3145$	1,312 / 9,046	7
E 6 NW	$\epsilon_{\max} = -2144$	410 / 2,829	5
SW	$\epsilon_{\max} = -3620$	472 / 3,255	2
SE	$\epsilon_{\max} = -2772$	146 / 1,007	5
NE	$\epsilon_{\max} = -1819$	971 / 6,693	1
C3-6 NW	$\epsilon_{\max} = -2318$	160 / 1,103	5
NE	$\epsilon_{\max} = -1741$	351 / 2,420	4
SW	$\epsilon_{\max} = -3214$	1,234 / 8,511	2
SE	$\epsilon_{\max} = -1110$	305 / 2,100	1
C3-9 N	$\epsilon_{\max} = -3063$	399 / 2,751	4
S	$\epsilon_{\max} = -1819$	543 / 3,744	3
C 3bas4 N	$\epsilon_{\max} = -2256$	127 / 876	7
S	$\epsilon_{\max} = -2191$	158 / 1,089	7
C 3-11 S	$\epsilon_{\max} = -3469$	224 / 1,544	6
E 9 N	$\epsilon_{\max} < -1195$	291 / 2,006	1
S	$\epsilon_{\max} = -1433$	559 / 3,854	1
C 3-4 N	$\epsilon_{\max} = -988$	289 / 1,995	2
S	$\epsilon_{\max} = -254$	28 / 193	5
C 3-1 NE	$\epsilon_{\max} = -2028$	530 / 3,654	5
SW	$\epsilon_{\max} = -1939$	159 / 1,096	7
SE	$\epsilon_{\max} = -1939$	664 / 4,578	6

Table 4-7: Summary of the stress computations based on minimum strain readings.

Specimens number and pond designation	Reference: strain in $\mu\epsilon$,	Equal load ksi / MPa	Number of unbroken wires
E 5 NW	$\epsilon_{\min} = -1196$	151 / 1,041	3
NE	$\epsilon_{\min} = -3031$	203 / 1,401	6
SW	$\epsilon_{\min} = -1215$	81 / 556	7
SE	$\epsilon_{\min} = -1133$	124 / 856	5
E 10 S	$\epsilon_{\min} = -2441$	1019 / 7023	7
E 6 NW	$\epsilon_{\min} = -1819$	348 / 2,399	5
SW	$\epsilon_{\min} = -2772$	362 / 2,496	2
SE	$\epsilon_{\min} = -861$	45 / 313	5
NE	$\epsilon_{\min} = -1819$	971 / 6,693	1
C3-6 NW	$\epsilon_{\min} = -387$	27 / 184	5
NE	$\epsilon_{\min} = -387$	78 / 538	4
SW	$\epsilon_{\min} = -1569$	603 / 4,158	2
SE	$\epsilon_{\min} = -1110$	305 / 2,100	1
C3-9 N	$\epsilon_{\min} = -2726$	355 / 2,448	4
S	$\epsilon_{\min} = -1819$	543 / 3,744	3
C 3bas4 N	$\epsilon_{\min} = -114$	6 / 44	7
S	$\epsilon_{\min} = -2046$	147 / 1,017	7
C 3-11 S	$\epsilon_{\min} = -3469$	224 / 1,544	6
E 9 N	$\epsilon_{\min} = -953$	232 / 1,600	1
S	$\epsilon_{\min} = -1433$	559 / 3,854	1
C 3-4 N	$\epsilon_{\min} = -324$	95 / 655	2
S	$\epsilon_{\min} = -254$	28 / 192	5
C 3-1 NE	$\epsilon_{\min} = -1151$	301 / 2,075	5
SW	$\epsilon_{\min} = -58$	5 / 33	7
SE	$\epsilon_{\min} = -1939$	664 / 4,578	6

4.6.3.4 Analysis of the results

4.6.3.3.1 Determination of the maximum possible stress

Parallel research [32] involved Slow Strain Rate Testing (SSRT) of specimens fabricated from the same type of tendon material that was used for these experiments. This involved precorrosion of tensile specimens such that localized corrosion, termed layer corrosion, resulted as illustrated schematically in Figure 4-11. The shape of these reduced cross section areas was similar to what occurred in the present specimens; but the depth over length ratio of the SSRT specimens ranged between 0.1 and 0.6 which was greater than for the present specimens (see section 4.3). This series of specimens, as well as a series of smooth ones, was tested in tension while polarized to $-1.30 V_{SCE}$. The corresponding averaged results are presented in Table 4-8.

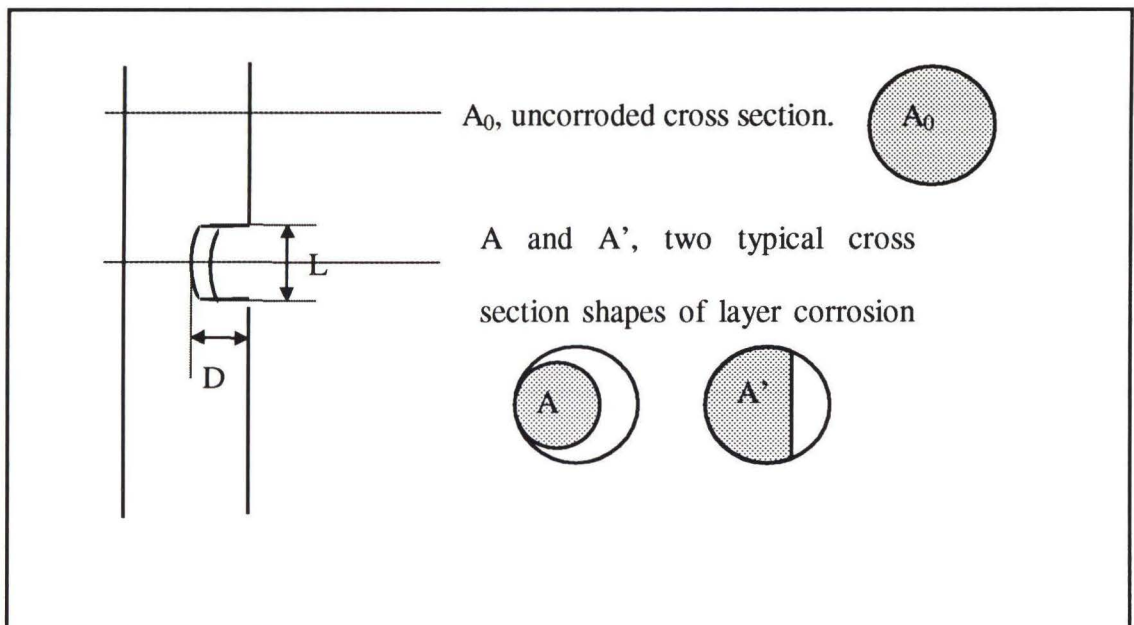


Figure 4-11: SSRT "layer corrosion" specimens.

Table 4-8: Results of SSRT experiments performed at $-1.3 V_{SCE}$.

Stress in MPa-ksi	Yield stress	Ultimate stress	Failure stress
Smooth specimens	1690 - 245	1967 - 285	1962 - 285
Layer corrosion Specimens	1513 - 219	1527 - 220	1527 - 222

The computations in the previous section (4.6.3.2) were performed for minimum wires cross sections where d/l in these zones was intermediate between those for smooth (nil) and layer corrosion type SSRT specimens. It is concluded that any computed stress (section 4.6.3.2) which exceeded the yield stress for smooth SSRT specimens (1690 MPa or 245 ksi) should be indicative of the wire having either 1) failed, 2) plastically deformed, or 3) transferred load to other wires. However, for SSRT specimens the stress range between yield and fracture was 0 and 16 percent of the yield stress for the layer corrosion and uncorroded cases, respectively. Thus, the probability of a wire failing if the actual stress were higher than the yield stress is high. Consequently, as these wires did not fail, computed stress values greater than the yield stress of smooth SSRT specimens probably did not reflect the actual stress state. Such situations were common, however, and are indicated by the shaded cells in Tables 4-6 and 4-7. A possible explanation for this is that these wires transferred load to the other, larger cross section ones.

4.6.3.3.2 Validity of the corrosion model

In order to check the validity of the corrosion model as applied to the specimen data for remaining wires and to determine trends, the number of specimens that exhibited computed stress values at the minimum wires cross section below and above 1690 MPa (245 ksi) was determined. The results are shown in Figure 4-12 for the case where $\epsilon_{\text{maximum}}$ was the computation reference and in Figure 4-13 for $\epsilon_{\text{minimum}}$. In the former case (Figure 4-12), most specimens with more than four remaining wires exhibited computed stress values below yield; however, in cases of less than four wires this stress commonly exceeded yield. If $\epsilon_{\text{minimum}}$ was the computation reference, the same trend resulted when the number of remaining wires exceeded four but results were mixed for fewer remaining wires (Figure 4-13).

These results are consistent with the theoretical model described in section 4.6.2 that projected equal load between wires at the early ages of corrosion. The preponderance of computed stress values which exceeded yield for more advanced corrosion levels (more than 3 severed wires) is also consistent with the theory from the standpoint that it predicts increased load transfer from the most corroded wire at advanced reduction of the tendon cross section area.

For most cases, the model also matches the physical aspect of severed wires whose failure area was corroded. It can be assumed that some failures occurred in the first 3 severed wires and that the failure surfaces corroded during further polarization. For specimens with the largest Ixt values a relatively large fraction of the load was probably transferred from wires of small cross section area, and this decreased the likelihood of

individual wire failures. The wire fractures that occurred during CP resulted for specimens that had been drilled before polarization. This setup caused relatively small corrosion zones (5 instead of up to 20 cm in length) with large cross section area reductions. This means that the ratio of the length of minimum cross section to the length of disbondment was probably high. Such a situation is projected to favor an equal load stress state which, in turn, promotes wire fracture once cross section is sufficiently reduced.

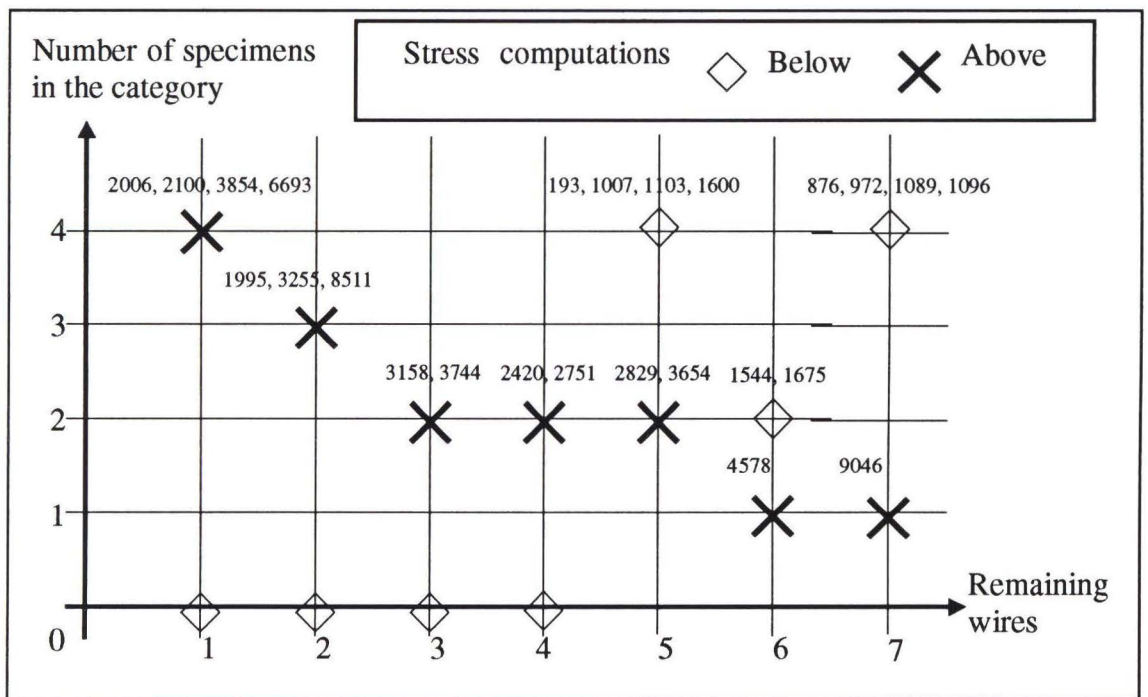


Figure 4-12: Number of specimens in each category for different numbers of remaining wires if $\epsilon_{\text{maximum}}$ is the computation reference.

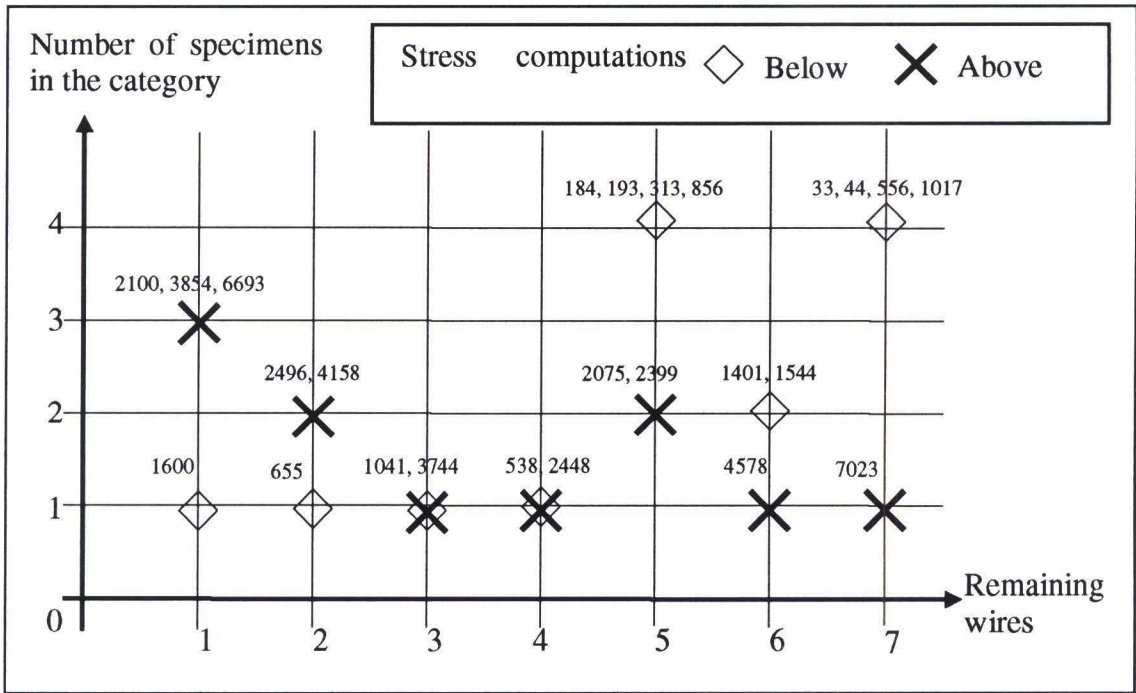


Figure 4-13: Number of specimens in each category for different numbers of remaining wires if $\epsilon_{\text{minimum}}$ is the computation reference.

4.7 Stress state evaluation charts

The model was used to develop reference charts which depict the magnitude of corrosion needed to cause fracture when the morphology of the wire at the location of smallest cross section is either smooth or intermediate between smooth and layer corrosion (described in section 4.6.3.3.1). Based on 1) the number of corroding wires, 2) the prestress of the tendon (5 to 70 percent of ultimate), 3) the number of remaining wires, and 4) the minimum cross section, the reference charts indicate if application of excessive CP on elements corroded to a given level should cause failure.

4.7.1 Simplified case where corrosion develops in one wire after another

If corrosion develops upon one wire at a time with the central one being the last to corrode, the equal load and equal stress models predict the same stress at times when the corroding wire either fractures or corrodes in two (all the unsevered wires are uncorroded). Alternately, during the period when a corroded wire is corroding and its cross section is reduced compared to the other wires, the equal load model predicts a higher stress level than the equal stress one. Table 4-9 shows the result of stress computations performed for different numbers of remaining uncorroded wires and different prestress levels for wires whose morphology in the minimum cross section zone is comparable with that of smooth SSRT specimens. Also, the maximum cross section area at each prestress which leads to yielding of the wire is indicated for both theories. When plastic deformation of the wire leads to yielding of the whole tendon, the result is indicated as a shaded cell. For wires whose minimum cross section zone morphology is intermediate between smooth and corrosion layer, the results are summarized in Table 4-10. In this case, the projection is conservative as the yield stress that was used is the average value obtained with layer corrosion SSRT specimens (see Figure 4-11).

Prestress in Mpa	7 wires left		6 wires left		5 wires left		4 wires left		3 wires left		2 wires left		1 wire left	
	Unsevered wires are uncorroded	Cross section area (mm2)	Unsevered wires are uncorroded	Cross section area (mm2)	Unsevered wires are uncorroded	Cross section area (mm2)	Unsevered wires are uncorroded	Cross section area (mm2)	Unsevered wires are uncorroded	Cross section area (mm2)	Unsevered wires are uncorroded	Cross section area (mm2)	Unsevered wires are uncorroded	Cross section area (mm2)
70% Ult 1300	1300	8.1	1513	9.5	1811									
			56.9	3.8										
65% Ult 1210	1210	7.6	1409	8.8	1689		2097							
					53.0	10.4								
60% Ult 1120	1120	7.0	1304	8.2	1560	9.8	1941							
					49.0	6.4								
55% Ult 1024	1024	6.4	1192	7.5	1426	9.0	1775							
					44.8	2.1								
50% Ult 931	931	5.8	1084	6.8	1297	8.2	1614	10.2	2136					
							40.8	8.5						
45% Ult 838	838	5.2	976	6.1	1167	7.3	1453	9.2	1923					
							36.7	4.4						
40% Ult 744	744	4.7	866	5.4	1036	6.5	1290	8.1	1707		2524			
							32.6	0.3						
35% Ult 652	652	4.1	759	4.8	908	5.7	1130	7.1	1496	9.5	2212			
									28.5	6.7				
30% Ult 558	558	3.5	650	4.1	777	4.9	967	6.1	1280	8.1	1893			
									24.4	2.6				
25% Ult 466	466	2.9	543	3.4	649	4.1	808	5.1	1069	6.8	1581	10.2	3031	
											20.4	9.0		
20% Ult 372	372	2.3	433	2.7	518	3.3	645	4.1	854	5.4	1262	8.1	2419	
											16.3	4.9		
15% Ult 280	280	1.8	326	2.0	390	2.5	485	3.1	642	4.1	950	6.1	1821	
											12.3	0.9		
10% Ult 186	186	1.2	217	1.4	259	1.6	322	2.0	427	2.7	631	4.1	1210	8.1
													8.1	8.1
5% Ult 93	93	0.6	108	0.7	130	0.8	161	1.0	213	1.4	315	2.0	605	4.1
													4.1	4.1

Any cell of the table may contain:
 1) Stress if all the remaining wires are uncorroded.
 2) Maximum section area (mm2) for yielding of the wire according to the equal load model.
 3-1) Maximum section area (mm2) of the corroding wire for yielding of the tendon according to the equal stress model.
 3-2) Maximum section area (mm2) of the tendon for yielding according to the equal stress model.

Example cell:

1)	2)
3-2)	3-1)

67

Shaded cells indicate cross section area of the corroded wire leading to onset of plastic deformation in the whole tendon.
 Uncorroded cross section areas are 10.4 mm2 for side wires and 11.4 mm2 for the central one.

Table 4-9: Stress level and critical cross section for different levels of prestress and cross section reduction when the zone of minimum cross section of the wire can be compared to a smooth SSRT specimen.

Prestress in Mpa	7 wires left		6 wires left		5 wires left		4 wires left		3 wires left		2 wires left		1 wire left	
	Unsevered wires are uncorroded	Cross section area (mm ²)	Unsevered wires are uncorroded	Cross section area (mm ²)	Unsevered wires are uncorroded	Cross section area (mm ²)	Unsevered wires are uncorroded	Cross section area (mm ²)	Unsevered wires are uncorroded	Cross section area (mm ²)	Unsevered wires are uncorroded	Cross section area (mm ²)	Unsevered wires are uncorroded	Cross section area (mm ²)
70% Ult 1300	1300	9.1	1513		1811									
	63.7	0.1												
65% Ult 1210	1210	8.5	1409	9.9	1689		2097							
			59.3	6.2										
60% Ult 1120	1120	7.8	1304	9.1	1560		1941							
			54.9	1.8										
55% Ult 1024	1024	7.2	1192	7.5	1426	10.0	1775							
					50.2	7.5								
50% Ult 931	931	6.5	1084	6.8	1297	9.1	1614							
					45.6	2.9								
45% Ult 838	838	5.9	976	6.1	1167	7.3	1453	10.3	1923					
							41.1	8.8						
40% Ult 744	744	5.2	866	5.4	1036	6.5	1290	9.1	1707					
							36.5	4.2						
35% Ult 652	652	4.6	759	4.8	908	5.7	1130	7.1	1496	10.7	2212			
									32.0	10.1				
30% Ult 558	558	3.9	650	4.1	777	4.9	967	6.1	1280	9.1	1893			
									27.3	5.5				
25% Ult 466	466	3.3	543	3.4	649	4.1	808	5.1	1069	7.6	1581			
									22.8	1.0				
20% Ult 372	372	2.6	433	2.7	518	3.3	645	4.1	854	5.4	1262	9.1	2419	
											18.2	6.9		
15% Ult 280	280	2.0	326	2.0	390	2.5	485	3.1	642	4.1	950	6.9	1821	
											13.7	2.3		
10% Ult 186	186	1.3	217	1.4	259	1.6	322	2.0	427	2.7	631	4.1	1210	9.1
													9.1	9.1
5% Ult 93	93	0.7	108	0.7	130	0.8	161	1.0	213	1.4	315	2.0	605	4.6
													4.6	4.6

Any cell of the table may contain:
 1) Stress if all the remaining wires are uncorroded.
 2) Maximum section area (mm²) for yielding of the wire according to the equal load model.
 3-1) Maximum section area (mm²) of the corroding wire for yielding of the tendon according to the equal stress model.
 3-2) Maximum section area (mm²) of the tendon for yielding according to the equal stress model.

Example cell:

1)	2)
3-2)	3-1)

Shaded cells indicate cross section area of the corroded wire leading to onset of plastic deformation in the whole tendon.

Uncorroded cross section areas are 10.4 mm² for side wires and 11.4 mm² for the central one.

Table 4-10: Stress level and critical cross section for different levels of prestress and cross section reduction when the

zone of minimum cross section of the wire can be compared to a layer corrosion SSRT specimen.

4.7.2 Application to tendons where corrosion developed in different wires at the same time.

If corrosion develops in different wires at the same time, the wire that fails first should still be the one with the smallest cross section area; however, load transfer may take place from the most corroded wire to the others. The magnitude of this transfer is not quantifiable in this case because of the multiplicity of factors involved (for example, tendon cross section area, cross section area of the different wires, length of the corrosion zone, length of the bond loss zone and distance between wire failures). Consequently, the only stress computation that could be performed was based on the equal load theory and, hence, is conservative. Accordingly, for the present specimens, even when $\epsilon_{\text{minimum}}$ was the reference, the computations gave stress values in the individual wires that were up to 3.6 times the average ultimate for smooth SSRT specimens (1967 MPa) for a wire that did not break (specimen E10 pond S).

Specimen E5 pond NW serves as an example whereby susceptibility to HE due to excessive CP could be investigated. The tendon in this case had three unsevered wires (Table 4-4); and the shape of the corrosion zones was intermediate between those of smooth and layer corrosion SSRT specimens in that the morphology was the same as for the layer type but with smaller d/l . Here, Table 4-10 applies. If the beam prestress is computed using $\epsilon_{\text{maximum}}$ (equivalent to a prestress of 40 percent of ultimate) failure is always predicted with just three remaining wires. However, the specimen in its final condition is predicted to retain its integrity (not fracture) upon application of excessive CP if the beam prestress is computed with $\epsilon_{\text{minimum}}$ (equivalent to a prestress of 13 percent

of ultimate). Treating this as corresponding to a prestress of 15 percent, it is seen that the maximum wire cross section area leading to failure of a tendon with three remaining wires is 4.1 mm^2 which is less than the minimum wire cross section that was actually present (5.9 mm^2). However, conservative diagnostics require that stress computations be based on the maximum strain reading.

The results of the present work may be used for field application to investigate the risk of brittle failure of prestressed concrete elements in association with excessive CP. In this regard the engineer should select a sample structural element representative of the most severe corrosion based upon visual observation or any other appropriate technique. Next, the residual pretension is either measured or a value assumed. For measurement, tendon gauges must be installed upon a tendon according to the protocol described in section 3.4.3. This location should be corrosion free for a minimum of three tendon twist lengths between the gauge and any corrosion zone in order to obtain a valid approximation of the uncorroded tendon strain. Then the tendon in question is detensioned, and the highest strain reading that is obtained is translated to a prestress. The stress analysis should be performed based upon the remaining unsevered wires. This is a conservative approach as a wire may carry load at some distance from where it severed. The smallest wire cross section area and the corrosion morphology of the wire are defined in this region. If the wire is smooth or if the morphology is intermediate between smooth and layer corrosion, projection of brittle failure is as indicated in Tables 4-9 and 4-10, respectively. In order to perform the analysis when the corrosion morphology of the wire at minimum cross

section is more acute (for example, pits with $d/l \geq 0.1$) additional tables have to be developed using the same model and data from ongoing parallel research [32]. If the corrosion level of the samples exceeds that for applying CP safely according to Tables 4-9 and 4-10, the evaluation should be extended to areas that exhibit a less severe corrosion level, and the sections for which failure is predicted replaced. It must be noted that the computation of longitudinal stress in unsevered wires does not take into account any service loads; and so the magnitude of these should be added to the prestress for a final assessment.

5. CONCLUSIONS

Based upon experiments involving sequential anodic and the cathodic polarization of pretensioned tendons in concrete, the following conclusions were reached:

- 1) Due to different experimental setups and polarized potentials, a relatively large range of cross section area reductions upon the corroded tendons were obtained; but corrosion morphology was generally the same and consisted of cross section area reductions with no sharp angles and d/l (depth over length ratio) rarely exceeding 6×10^{-2} . Moreover, autopsies of the specimens after testing revealed numerous wires that either fractured or corroded in two during the anodic polarization with only a small fraction having fractured during CP.
- 2) The average level of prestress in the tendons was less than 22 percent of the ultimate strength, and this was not significantly affected by polarization. This low value may have been a contributing factor to the finding that only a few fractures were brittle.
- 3) A corrosion model was developed from theoretical considerations and considering the experimental data. Coupled with data from parallel research, stress state evaluation charts were developed for two typical corrosion morphologies. Based on the number

of severed and corroded wires, the prestress level, and the minimum cross section, a method was established to determine if application of excessive CP to corroded prestressed tendons should cause failure.

APPENDIX

Computation of strain difference between side and center wires if a tendon is stretched with fixed grips:

For an unstressed tendon, consider that the spiral repeat length of a side wire is D_0 and the corresponding length of the central wire is L_0 . Further, let θ be the angle of twist and r the distance between the center of the center wire and that of the side wires. For a 11.1 mm (7/16 in.) diameter tendon this yields $r = 1.82 + 1.90 \text{ mm} = 3.72 \text{ mm}$.

Measurements on tendons from the present specimens indicated that the length of the straight central wire corresponding to a complete revolution of the spiraled wires ($\theta = 2\pi$) was $L_0 = 160 \text{ mm}$. Thus, the corresponding length of the spiraled wire is

$$D_0 = \int_{z=0}^{z=160} \sqrt{1 + \left(\frac{\partial x}{\partial z}\right)^2 + \left(\frac{\partial y}{\partial z}\right)^2} \times dz, \quad \text{A1)}$$

where $x = r \cos \theta$, $y = r \sin \theta$, and $z = 160 \times \theta / (2\pi)$. Thus, $x = r \cos (2\pi z/160)$ and $y = r \sin (2\pi z/160)$ which yields $(dx/dz) = -2\pi r/160 \times \sin \theta$ and $(dy/dz) = 2\pi r/160 \times \cos \theta$.

Substituting the two last equalities into A1) gives

$$D_0 = \int_{z=0}^{z=160} \sqrt{1 + \left(\frac{2\pi \times r}{160}\right)^2} \times dz = 160 \times \sqrt{1 + \left(\frac{2\pi \times r}{160}\right)^2} \approx 161.70 \text{ mm, and}$$

so $D_0 = 1.01 \times L_0$ for an unstressed tendon.

As an example, if $\Delta \epsilon_{\text{side}} = \Delta D/D_0 = 9000 \mu\epsilon$ and $E = 207 \text{ GPa}$, then

$$\sigma_{\text{side}} = \epsilon_{\text{side}} \times E = 1,863 \text{ MPa.}$$

Thus, $\Delta D = D_0 \times .009 = 161.7 \times .009 = 1.45 \text{ mm}$, and $D = D_0 + \Delta D = 161.7 + 1.45$

$$= 163.15 \text{ mm} = L \times \sqrt{1 + \left(\frac{2\pi \times r}{L}\right)^2} \text{ or upon rearranging}$$

$$L = \sqrt{(D^2 - 4(\pi \times r)^2)} = 161.47 \text{ mm.}$$

Thus, $\Delta \epsilon_{\text{center}} = \Delta L/L_0 = 9170 \mu\epsilon$, and $\Delta \epsilon_{\text{center}} = \Delta \epsilon_{\text{side}} \times 1.019$.

Using the same technique, ϵ_{center} was computed for other values of ϵ_{side} , and these values are summarized in Table A-1. This table also contains the percentage of variation (k) between the two strains, which ranges from 1 to 1.86 %.

As the error in the strain readings was considered to be greater than 2 % (see section 4.1), the measured strain upon a spiraled wire can be assumed to apply also to the central wire.

ϵ_{side}	9000	8000	7000	6000	5000	4000	3000	2000	1000
ϵ_{center}	9167.6	8148.3	7127.2	6105.8	5084.6	4063.3	3042.1	2020.7	1010
k (%)	1.862	1.854	1.817	1.764	1.692	1.582	1.403	1.035	1

Table A-1: Correspondance between values of ϵ_{side} and ϵ_{center} .

REFERENCES

- [1]: Federal Highway Administration, Highway Bridge Replacement and Rehabilitation Program 1991, Tenth Report of the Secretary of Transportation to the United States Congress, June 1991.
- [2]: B. Isecke and J. Mietz, "The Risk of Hydrogen Embrittlement in High-Strength Pre-stressing Steels Under Cathodic Protection", Steel Research, volume 64, Number 1, 1993, p 97.
- [3]: R. N. Parkins, M. Elices, V. S. Galvez and L. Caballero, Corrosion Science, Volume 22, 1982, p 379.
- [4]: V.S. Galvez, L. Caballero and M. Elices, ASTM STP 866, American Society for Test. And Materials, 1985, p 428.
- [5]: W. T. Scannell and W.H. Hartt, Materials Performance, volume 26(12), 1987, p 32.
- [6]: J. Wagner, W. Young, S. Scheirer and P. Fairer, "Cathodic Protection Developments for Prestressed Concrete Components", Report No. FHWA-RD-92-056, Federal Highway Administration, Washington, DC, March 1993.
- [7]: S. Kliszowski and W. H. Hartt, "Mechanical Properties and Fracture Strength of Cathodically Polarized Prestressing Wire", Corrosion /96, Denver, Paper Number 315, March 1996.

- [8]: E. G. Nawy, "Reinforced Concrete, A Fundamental Approach", Prentice Hall International Series in Civil Engineering and Engineering Mechanics, Second Edition, New Jersey, 1990.
- [9]: D. A. Jones, Principles and Prevention of Corrosion, Macmillan Publishing Company, New York, 1992, p 52.
- [10]: K. W. J. Treadaway, "Corrosion of Pre-stressed Steel Wire in Concrete", Br. Corrosion Journal, Volume 6, March 1971, pp. 66-72.
- [11]: D. A. Hausmann, Materials Protection, October 1969, pp. 23-25.
- [12]: D. A. Jones, Principles and Prevention of Corrosion, Macmillan Publishing Company, New York, 1992, p93.
- [13]: W. H. Hartt, "A Critical Evaluation of Cathodic Protection for Pre-stressing Steel in Concrete", Corrosion of Reinforcement in Concrete, Society of Chemical Industry, Elsevier Applied Science, London and New York, May 1990, pp. 515-523.
- [14]: NACE, Standard Recommended Practice, "Cathodic Protection of Reinforcing Steel in Atmospherically Exposed Concrete Structures", NACE Standard, RP 0290-90, National Association of Corrosion Engineers, Houston, Texas.
- [15]: D. A. Jones, Principles and Prevention of Corrosion, Macmillan Publishing Company, New York, 1992, p 248.
- [16]: D. A. Jones, Principles and Prevention of Corrosion, Macmillan Publishing Company, New York, 1992, p 340.

- [17]: S. Kliszowski, "Hydrogen Embrittlement Susceptibility of Pre-stressing Steel", Master's Thesis, Department of Ocean Engineering, Florida Atlantic University, February 1994.
- [18]: ASTM Committee G-1, Subcommittee G 01.05, "Standard Guide for Examination and Evaluation of Pitting Corrosion", April 1994.
- [19]: J. F. Elliott, "Monitoring Pre-stressed Structures", Civil Engineering, July 1996, p 61-63.
- [20]: C. Dale Buckner, State-of-the-Art Report, "A Review of Strand Development Length for Pre-tensioned Concrete Members", PCI Journal, March-April 1995, p84-101.
- [21]: E. G. Nawy, Pre-stressed Concrete, A Fundamental Approach, Prentice Hall International Series in Civil Engineering and Engineering Mechanics, 1989, p 65.
- [22]: A. Owens, "In Situ Stress Determination Used in Structural Assessment of Concrete Structures", Strain, November 1993.
- [23]: ACI Committee 318, "Building Code Requirements for Reinforced Concrete (ACI318-89)", American Concrete Institute, Detroit, MI, 1989.
- [24]: AASHTO, "Standard Specifications for Highway Bridges", 15th edition, American Association of State Highway and Transportation Officials, Washington D. C., 1992.
- [25]: P. Zia and T. Mostafa, "Development Length of Pre-stressing Strands", PCI Journal, volume 22, Number 5, September-October 1977, pp. 54-65.

- [26]: L. Martin and N. L. Scott, "Development of Pre-stressing Strand in Pre-tensioned Members", ACI Journal, Volume 73, Number 8, August 1976, pp. 453-456.
- [27]: J. H. Deatherage, E. G. Burdette and C. K. Chew, "Development Length and Lateral Spacing Requirements of Pre-stressing Strand for Pre-stressed Concrete Bridge Girders", PCI Journal, Volume 39, Number 1, January-February, 1994 pp. 70-83.
- [28]: W. Hartt, E. Joubert and S. Kliszowski, "Long Term Effect of Cathodic Protection on Pre-stressed Concrete Bridge Components", Florida Atlantic University, FHWA Interim Report, October 1992 to March 1995.
- [29]: K. Hoffmann, "An Introduction to Measurements Using Strain Gauges", Hottinger, Baldwin Messtechnik GmbH, Darmstadt, 1989.
- [30]: E. Joubert, "Pre-stressing Steel to Concrete Bond Degradation due to Cathodic Polarization", Master's Thesis, Department of Ocean Engineering, Florida Atlantic University, December 1995.
- [31]: Measurement Group Information Bulletin #219, "Surface Preparation for Strain Gauge Installation".
- [32]: A. L. Stauder, Unpublished Research, Department of Ocean Engineering, Florida Atlantic University, 1997.

